Decentralized Formation and Attitude Control of Spacecraft:

Decentralized Spacecraft Assembly of Megastructures in an Elliptic Orbit

Submitted in partial fulfillment of the requirements
of the degree of

Bachelor of Technology

by

Aaron John Sabu
(Roll No. 170070050)

Supervisor:
Prof. Dwaipayan Mukherjee

Department of Electrical Engineering
INDIAN INSTITUTE OF TECHNOLOGY BOMBAY
Spring 2021

Dedicated to God Almighty for everything in my life,
particularly my beloved parents and sister,
my institution, advisor, and instructors,
and my friends and supporters.

Declaration

I declare that this written submission represents my ideas in my own words, and where others' ideas or words have been included, I have adequately cited and referenced the original sources. I also declare that I have adhered to all principles of academic honesty and integrity and have not misrepresented, fabricated, or falsified any idea/data/fact/source in my submission. I understand that any violation of the above will be cause for disciplinary action by the Institute and can also evoke penal action from the sources that have not been adequately cited or from whom proper permission has not been taken when needed.

Date: 2021-04-12

Aaron John Sabu

Roll No. 170070050

Acknowledgments

I wish to record a deep sense of gratitude to my supervisor, **Prof. Dwaipayan Mukherjee** for his valuable guidance and constant support throughout the B.Tech project. He was always available at a very short time's notice, accepted my ignorance with an open heart, and was willing to spend time advising and providing feedback. I firmly believe that he has had an enormous role in transforming this project into much more than just an academic pursuit.

Secondly, I am incredibly grateful to my father, **Dr. Sabu John**, my mother, **Mrs. Jessy Sabu John**, and my sister, **Dr. Priscilla Thankam Sabu**, for supporting me in every way possible throughout the progress of the project. I firmly believe that achieving goals would have been a matter of great worry in these challenging times if not for their cooperation and support.

Finally, I am thankful to everyone who has positively impacted my life and undergraduate career, from instructors who have personally guided me throughout my studies to my friends and peers who have never failed to inspire me.

Abstract

The curiosity of humankind has led them to investigate the entire universe. However, human-made technology is not always at par with human curiosity, and an example is the inability to send large telescopes to outer space despite the need to do so for higher resolution and less atmospheric interference. We develop a framework for decentralized spacecraft formation flying and in-orbit construction such that a large telescope can be built in an elliptic orbit around the earth using multiple spacecraft. We split this problem into four steps for converging the position and attitude of each spacecraft at predefined values around a central spacecraft. Each spacecraft performs attitude synchronization with its neighbors to match its three orientational degrees of freedom as a parabolic mirror. Finally, we conclude the research with a description of the future scope of this work and the possibility of using specific techniques to achieve superior results.

Contents

List of Figures

List of Abbreviations

ACS . . . . . Attitude Control System

AOCS . . . . . Attitude and Orbit Control System

AR&D . . . . . Autonomous Rendezvous and Docking

cm . . . . . center of mass

CA . . . . . Clear Aperture

CWH . . . . . Clohessy-Wiltshire-Hill [equations]

GNC . . . . . Guidance, Navigation, and Control

IFMEA . . . . . Intra-Formation Mutual Exchange Algorithm

JWST . . . . . James Webb Space Telescope

LVLH . . . . . Local-Vertical-Local-Horizontal [frame]

OAP . . . . . Off-Axis Paraboloid(al)

ROA . . . . . Reference Optical Axis

STM . . . . . State Transition Matrix

TH . . . . . Tschaner-Hempel [equations]

YA . . . . . Yamanaka-Ankersen [solution]

ZSP . . . . . Zavlanos-Spesivtsev-Pappas [auction algorithm]

Chapter 1

Introduction

1.1 Background

Modularity has been a common feature in building structures throughout history. Here on earth, we have built them from bricks and mortar, and we have constructed structures in space from specially-built compartments. However, the length (longest dimension) of the largest structure we have ever constructed in space, the International Space Station, is much smaller than the height (longest dimension) of the Kushan stupa of Kanishka that dates back to the 2nd century AD. Constructing a megastructure in space has demanded much more resources than on the ground in terms of fuel and workforce .

Similarly, we have been able to deploy large telescopes both on earth (Gran Telescopio Canarias, Keck 1) and space (Hubble Space Telescope, the Great Observatories program). It is more favorable to place telescopes in space to counter artificial glow from light pollution and the decrease in resolving power due to air turbulence. Moreover, the bigger the telescope is, the better its resolving power and its light-gathering ability. However, we have always been limited in our capability of sending large telescopes to space due to rocket payload limitations.

Large telescopes can be deployed in space by building the telescopes in orbit using smaller

modules that host the telescope's segments. Robotic arms have been used for similar activities in the past. However, this imports more complexity into the problem due to the dynamics of the arms. Also, in the quest to prevent collisions and provide a safe work environment, it may be required to conduct the mission over several stages in a more extended period, resulting in the utilization of more resources and the subsequent increase in expenditure.

As a result of the problems mentioned above in construction using robotic arms, researchers have been looking into the possibility of self-assembly of spacecraft formations in orbit. We derive motivation for this research based on the similar work done by Foust et al. (2017) on autonomous rendezvous and docking (AR&D) of spacecraft to build a telescope in orbit. However, this research has dealt with construction in a circular orbit, collision avoidance is not considered explicitly in the problem, and there is little discussion on each spacecraft's attitude dynamics. We develop a simple framework that breaks down the spacecraft formation problem into four steps to collectively solve the problem of converging to a neighborhood, self-arranging into a predefined configuration, and attaining configuration-based orientations.

1.2 Motivation

- The maximum size possible for a large telescope in outer space is constrained by the size of the payload fairing and subsequently the size of the rocket.
- It is not recommendable to use robotic arms for in-orbit construction due to the extra complexity involved in controlling the motion of the arms. Moreover, using robotic arms can significantly decrease the scalability of the process.
- Centralized methods such as a central spacecraft dictating target locations cannot be scalable for large formations due to the latency in communication and similar issues.
- Present techniques available for decentralized spacecraft formation involve complex algorithms that do not necessarily prevent collisions.

These reasons demand developing a simple but reasonably practical framework for decentralized spacecraft formations in orbit.

1.3 Research Objectives and Problem Statement

This thesis presents a four-stage framework that can be implemented to construct a space telescope in an elliptic orbit around the earth. We consider a central spacecraft that hosts the on-axis segment of a large parabolic telescope and multiple spacecraft, each of which hosts an off-axis segment. Each spacecraft forms a communication network after its ejection in a mission-specific orbit with neighboring spacecraft and subsequently converges at a specific point of 'unorganized pre-assembly'. These locations may be mismatched for some or all spacecraft due to the differentiation in the physical configuration that arises from the variations of off-axis parabolic mirrors. Hence, mismatched spacecraft are re-assigned to matching locations while avoiding collisions in the process, leading to the 'organized pre-assembly' stage. The spacecraft will simultaneously synchronize their attitudes with neighboring spacecraft in the local frame of reference. Finally, the spacecraft form an assembly and form the space telescope using a technique similar to the tether-based docking (Foust et al. (2017)) to join with their neighbors. The concept for intermediate pre-assembly followed by the final assembly has been inspired from work by Chen et al. (2017) as depicted in Fig. 1.2 although the overall problem dealt with the mentioned research is not aligned with our problem.

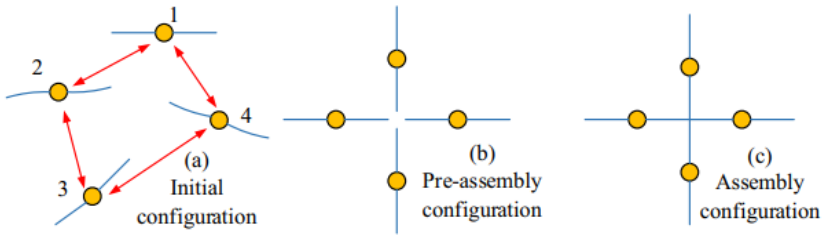

Figure 1.1: Configuration Transformations (Chen et al. (2017))

The above-mentioned steps can be described as a flowchart in the following manner:

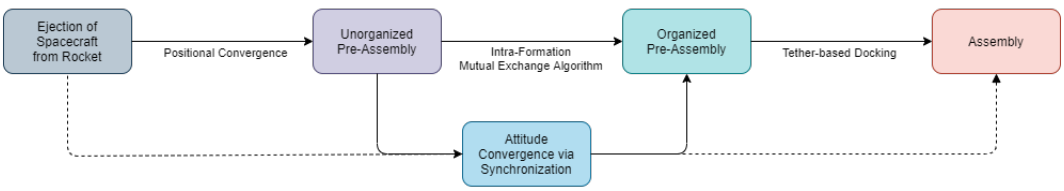

Figure 1.2: Complete Flowchart

1.4 Thesis outline

The subject matter of the thesis is presented in the following chapters:

- ✓ Chapter 2 provides an introduction into concepts from spacecraft dynamics, including motion in non-inertial frames and the conversion of independent variables.
- ✓ Chapter 3 describes basic principles of translation of spacecraft in non-inertial frames and the application of certain algorithms to optimize such transfer for multiple agents.
- ✓ Chapter 4 incorporates the features of parabolic mirrors to calculate the final position and attitude of the spacecraft and formulates an algorithm to suitably translate the spacecraft.
- ✓ Chapter 5 applies recent developments in attitude synchronization to converge the orientations of the spacecraft to values defined by their position and physical configuration.
- ✓ Chapter 6 provides concluding remarks on the research and the directions in which it can further be progressed.

Chapter 2

Preliminary Knowledge on Spacecraft Dynamics

2.1 Introduction

The configuration of a rigid spacecraft is defined by six elements with respect to a predetermined frame of reference, three representing its position in three-dimensional space and three representing its orientation with respect to the axes of the reference frame. This chapter provides insight regarding the importance of orbital parameters for position determination as well as the control inputs for smaller variations in the position. It also intends to provide the reader an understanding of how a spacecraft tends to move with respect to a frame of reference that is fixed with respect to a neighboring spacecraft. This relative motion will be used to describe motion through the rest of this research.

2.2 The Spacecraft in Consideration

We will consider each spacecraft of the telescope assembly to be similar in basic structure to a satellite that minimally consists of a central body, solar arrays, antenna tower(s), and controller and attitude sensors. The spacecraft will include a propulsion system, either chemical or ion-based, to vary its positional trajectory and/or its attitude at calculated intervals. The AOCS hardware of the spacecraft may also include momentum wheels, horizon sensors, sun sensors, gyroscopes, etc. to measure and fine-tune its attitude. Additionally the spacecraft will host a segment of the parabolic telescope. A simplistic model of the spacecraft is depicted in Fig. 2.1. The spacecraft design depicts the use of redundant thrusters. Such extra thrusters generally increase the reliability of the spacecraft control system and provide backup in the case of thruster failure (Jin et al. (2006)). Moreover, tethers are wound up at a side of the spacecraft and are unwound to dock with neighboring spacecraft after the organized pre-assembly stage is attained.

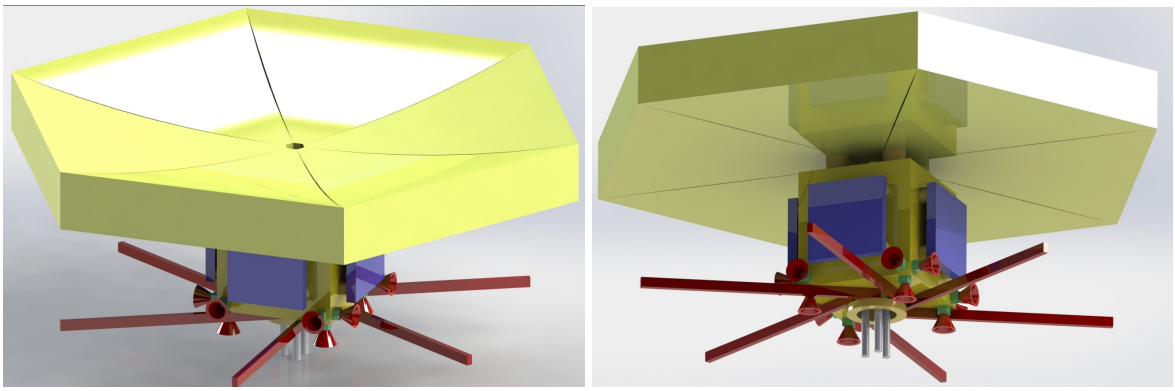

(a) Dimetric View (b) Bottom Dimetric View

Figure 2.1: The Spacecraft in Consideration

2.3 Orbital Parameters

According to Sidi (1997), an inertial reference frame can be defined for an earth-orbiting spacecraft as follows: the origin is at the center of mass of the Earth; the **Z** axis is the axis of rotation of the Earth in the positive direction; the **X** axis is the *vernal equinox* vector formed by the intersection of the equatorial plane with the ecliptic plane[1] at 22.5°; and the **Y** axis is defined by completing the orthogonal right-handed system. The X axis intersects the celestial sphere at

[1] the plane of Earth's orbit around the Sun

the *vernal point* or *first point of the Aries* (Υ).

The classical orbit parameters of the elliptic orbit of a spacecraft around the Earth are given by a vector $\boldsymbol{\alpha}$. The component of this vector, as represented in Figure 2.2, are defined as follows:

- a, the *semi-major axis* of the ellipse,
- e, the *eccentricity* of the ellipse,
- i, the *inclination*, i.e., the angle made between the orbit and the earth's equatorial plane,
- Ω, the *right ascension* of the ascending node, i.e., the angle from a specific reference direction (origin of longitude) to the direction of the ascending node of the orbit, as measured in a specified reference plane[2],
- ω, the *argument of perigee*, i.e., the angle between the radius vector of the moving body ($\boldsymbol{r}$) and the the radius vector of the perigee ($\boldsymbol{r_P}$), and
- $M = n(t - t_0)$, the mean anomaly[3]

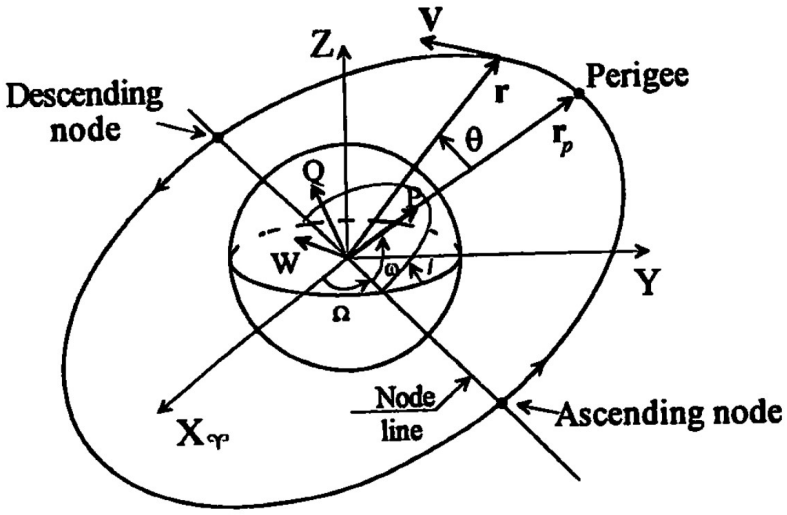

Figure 2.2: Classical Elliptic Orbit Parameters (Sidi (1997))

Bloise et al. (2017) introduce the concept of the Local-Vertical-Local-Horizontal (LVLH) frame of reference, usually coincident with the center of mass of the target (which is the central spacecraft in our case), as depicted in Fig. 2.3. The motion of other bodies in this frame of reference

[2]For geocentric orbits, Earth's equatorial plane is the reference plane, and the First Point of Aries ($\boldsymbol{X}_\Upsilon$) is the origin of longitude

[3]n is the mean motion, the angular speed required for a body to complete one orbit, assuming constant speed in a circular orbit which completes in the same time as the variable speed, elliptical orbit of the actual body

is defined in terms of certain non-linear relations that depend on the eccentricity of the orbit. In general, these relations are referred to as the Euler-Hill equations.

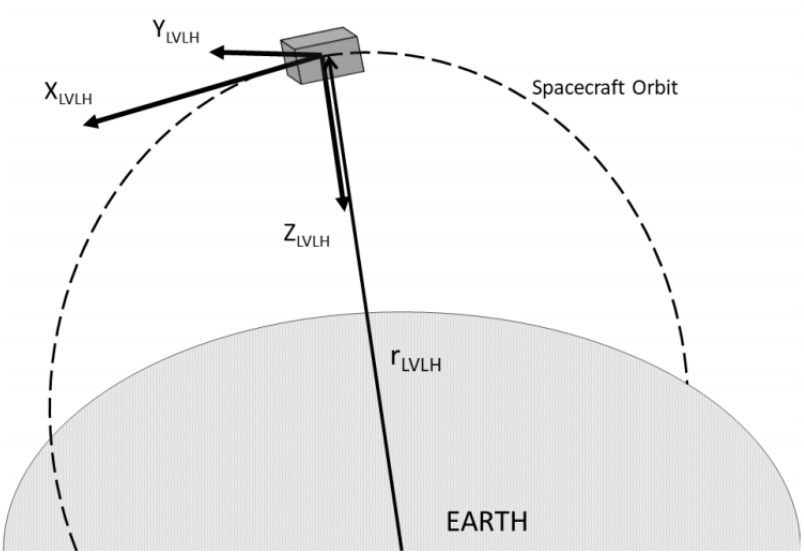

Figure 2.3: Local-Vertical-Local-Horizontal (LVLH) Frame (Bloise et al. (2017))

2.4 Relative Motion of Nearby Objects

2.4.1 Euler-Hill Equations

When two satellites move in almost identical orbits and are very near to each other, we may define a non-inertial coordinate frame of reference with the origin fixed at and moving with the center of mass of one satellite. The coordinates of the other satellite are calculated in this moving coordinate frame, hence describing the relative motion of satellites in neighboring orbits. These equations of motion of the second satellite with respect to the first are called the *Euler-Hill equations*. This formulation can be used to solve problems involving the relative motion of neighboring satellites such as the rendezvous problem between two spacecraft.
Consider two satellites at $\boldsymbol{r_1}$ and $\boldsymbol{r_2}$. Let $\boldsymbol{\rho} = \boldsymbol{r_1} - \boldsymbol{r_2}$. From the law of universal gravitation,

$$\ddot{\boldsymbol{r}}_{\mathbf{1}} = -\mu \boldsymbol{r_1}/r_1^3 \tag{2.1a}$$

$$\ddot{\boldsymbol{r}}_{\mathbf{2}} = -\mu \boldsymbol{r_2}/r_2^3 + \boldsymbol{f} \tag{2.1b}$$

This can be used to form a differential equation in $\boldsymbol{\rho}$ (Sidi (1997)) as:

$$\ddot{\boldsymbol{\rho}} = \frac{\mu}{r_1^3}\left(-\boldsymbol{\rho} + 3(\boldsymbol{r_1}\cdot\boldsymbol{\rho})\frac{\boldsymbol{r_1}}{r_1^2}\right) + \boldsymbol{f} + O(r^2) \tag{2.2}$$

Alfriend et al. (2009) develop the linearization of this formulation as developed by Clohessy and Wiltshire. The nonhomogeneous forms of these equations are given as:

$$\ddot{x} - 2n\dot{y} - 3n^2x = f_x \tag{2.3a}$$

$$\ddot{y} + 2n\dot{x} = f_y \tag{2.3b}$$

$$\ddot{z} + n^2z = f_z \tag{2.3c}$$

In the absence of the force $\boldsymbol{f}$, we get:

$$\ddot{x} - 2n\dot{y} - 3n^2x = 0 \tag{2.4a}$$

$$\ddot{y} + 2n\dot{x} = 0 \tag{2.4b}$$

$$\ddot{z} + n^2z = 0 \tag{2.4c}$$

Solving these equations gives us:

$$\boldsymbol{x}(t) = e^{A(t-t_0)}\boldsymbol{x}(0) \tag{2.5}$$

where, provided $c_{nt} = cos(nt)$ and $s_{nt} = sin(nt)$,

$$e^{At} = \begin{bmatrix} 4-3c_{nt} & 0 & 0 & \frac{s_{nt}}{n} & \frac{2}{n}-\frac{2c_{nt}}{n} & 0 \\ -6nt+6s_{nt} & 1 & 0 & -\frac{2}{n}+\frac{2c_{nt}}{n} & \frac{4s_{nt}}{n}-3t & 0 \\ 0 & 0 & c_{nt} & 0 & 0 & \frac{s_{nt}}{n} \\ 3ns_{nt} & 0 & 0 & c_{nt} & 2s_{nt} & 0 \\ -6n+6nc_{nt} & 0 & 0 & -2s_{nt} & -3+4c_{nt} & 0 \\ 0 & 0 & -ns_{nt} & 0 & 0 & c_{nt} \end{bmatrix} \tag{2.6}$$

This solution is commonly referred to as the Clohessy-Wiltshire-Hill (CWH) equations.

2.4.2 Tschauner-Hempel Equations

Considering that the space telescope will be built in low earth orbit, the orbit of each spacecraft is elliptic rather than circular due to which the CWH solution breaks down and it is required to formulate the relative equations of motion for the secondary spacecraft with respect to the primary one considering the eccentricity of the orbit. In fact, according to Fehse (2003), though they depend only on the initial state, orbit angular frequency, and time, the CWH equations are only accurate within about 30 km of the origin of the frame due to the linearization.
Unlike circular orbits, the choice of the independent variable being either time or true anomaly leads to different forms of the equations of motion for elliptic orbits. Time-explicit solutions such as that by Melton (2000) are attractive since Kepler's equation need not be solved to produce results at specified points of time. However, true-anomaly-based solutions prove advantageous especially near the perigee and are more suitable for long-term motion prediction for elliptic orbits. Moreover, using truncated approximations, it is possible to represent the true anomaly in terms of time and hence convert the true-anomaly-based STM into an approximate time-explicit STM. For this purpose, we look into the Tschauner-Hempel equations (Tschauner and Hempel (1964)):

$$\bar{x}'' = \frac{3}{k}\bar{x} + 2\bar{y}' \tag{2.7a}$$

$$\bar{y}'' = -2\bar{x}' \tag{2.7b}$$

$$\bar{z}'' = -\bar{z}' \tag{2.7c}$$

Here, $(\cdot)'$ and $(\cdot)''$ indicate, respectively, the first and second derivatives with respect to f, the true anomaly, and $k = 1 + e\cos f$.

2.4.2.1 Yamanaka-Ankersen Solution

Yamanaka and Ankersen (2002) develop a solution for the homogeneous version of Tschauner-Hempel equations without considering the force $\boldsymbol{f}$ that includes disturbance accelerations $\boldsymbol{d}$ and/or control accelerations $\boldsymbol{u}$. The solution is computed separately for in-plane (x and z axes) and out-of-plane (y axis) motions.[4] Moreover, the state transition matrix is calculated in two steps: first to convert the independent variables and next to propagate the initial state to a final

[4]The paper exchanges axes without the loss of generality.

state. Given the true initial values as $\boldsymbol{r}_0$ and $\boldsymbol{v}_0$, and $\tilde{\boldsymbol{r}}_i = [\tilde{x}_i, \tilde{y}_i, \tilde{z}_i]$ and $\tilde{\boldsymbol{v}}_i = [\tilde{v_x}_i, \tilde{v_y}_i, \tilde{v_z}_i]^T$, the true final values $\boldsymbol{r}_t$ and $\boldsymbol{v}_t$ can be calculated in the following steps.

The true initial values ($\boldsymbol{r}_0$) are converted into the transformed initial values ($\tilde{\boldsymbol{r}}_0$) as (Yamanaka and Ankersen (2002)):

$$\tilde{\boldsymbol{r}}_0 = \rho \boldsymbol{r}_0 \tag{2.8a}$$

$$\tilde{\boldsymbol{v}}_0 = -e \sin\theta \boldsymbol{r}_0 + \frac{1}{k^2 \rho} \boldsymbol{v}_0 \tag{2.8b}$$

The pseudoinitial values ($\bar{\boldsymbol{r}}_0$) can be calculated from the transformed initial values ($\tilde{\boldsymbol{r}}_0$) as:

$$\begin{bmatrix} \bar{x}_0 \\ \bar{z}_0 \\ \bar{v_x}_0 \\ \bar{v_z}_0 \end{bmatrix} = \frac{1}{1-e^2} \begin{bmatrix} 1-e^2 & 3es(\frac{1}{\rho}+\frac{1}{\rho^2}) & -es(1+\frac{1}{\rho}) & -ec+2 \\ 0 & -3s(\frac{1}{\rho}+\frac{e^2}{\rho^2}) & s(1+\frac{1}{\rho}) & c-2e \\ 0 & -3(\frac{c}{\rho}+e) & c(1+\frac{1}{\rho})+e & -s \\ 0 & 3\rho+e^2-1 & -\rho^2 & es \end{bmatrix}_{\theta_0} \begin{bmatrix} \tilde{x}_0 \\ \tilde{z}_0 \\ \tilde{v_x}_0 \\ \tilde{v_z}_0 \end{bmatrix} \tag{2.9a}$$

The transformed final values ($\tilde{\boldsymbol{r}}_t$) can be calculated from the pseudoinitial values ($\bar{\boldsymbol{r}}_0$) as:

$$\begin{bmatrix} \tilde{x}_t \\ \tilde{z}_t \\ \tilde{v_x}_t \\ \tilde{v_z}_t \end{bmatrix} = \begin{bmatrix} 1 & -c(1+\frac{1}{\rho}) & s(1+\frac{1}{\rho}) & 3\rho^2 J \\ 0 & s & c & (2-3esJ) \\ 0 & 2s & 2c-e & 3(1-2esJ) \\ 0 & s' & c' & -3e(s'J+\frac{s}{\rho^2}) \end{bmatrix} \begin{bmatrix} \bar{x}_0 \\ \bar{z}_0 \\ \bar{v_x}_0 \\ \bar{v_z}_0 \end{bmatrix} \tag{2.10a}$$

The two steps for the in-plane axes are merged into one for the out-of-plane transformation:

$$\begin{bmatrix} \tilde{y}_t \\ \tilde{v_y}_t \end{bmatrix} = \frac{1}{\rho_{\theta-\theta_0}} \begin{bmatrix} c & s \\ -s & c \end{bmatrix}_{\theta-\theta_0} \begin{bmatrix} \tilde{y}_0 \\ \tilde{v_y}_0 \end{bmatrix} \tag{2.11a}$$

The transformed final values ($\tilde{\boldsymbol{r}}_t$) are converted back into the true final values ($\boldsymbol{r}_t$) as:

$$\boldsymbol{r}_t = \frac{1}{\rho} \tilde{\boldsymbol{r}}_t \tag{2.12a}$$

$$\boldsymbol{v}_t = k^2 (e \sin\theta \tilde{\boldsymbol{r}}_t + \rho \tilde{\boldsymbol{v}}_t) \tag{2.12b}$$

In the above relations, the symbols are defined as: $\rho = 1 + e\cos\theta$, $s = \rho\sin\theta$, $c = \rho\cos\theta$, $s' = \cos\theta + e\cos 2\theta$, $c' = -(\sin\theta + e\sin 2\theta)$, $J = k^2(t - t_0)$, and $k^2 = h/p^2$.

The entire state transition matrix formed by the merging and multiplying the above mentioned matrices will be represented as $\Phi(f)$, and when converted to time coordinates, $\Phi(t)$. Furthermore, $\Phi(t)$ may be split into four 3×3 matrices as:

$$\Phi(t) = \begin{bmatrix} \Phi_{rr}(t) & \Phi_{r\dot{r}}(t) \\ \Phi_{\dot{r}r}(t) & \Phi_{\dot{r}\dot{r}}(t) \end{bmatrix} \tag{2.13}$$

such that:

$$\boldsymbol{r}_t = \Phi_{rr}(t)\boldsymbol{r}_0 + \Phi_{r\dot{r}}(t)\dot{\boldsymbol{r}}_0 \tag{2.14a}$$

$$\dot{\boldsymbol{r}}_t = \Phi_{\dot{r}r}(t)\boldsymbol{r}_0 + \Phi_{\dot{r}\dot{r}}(t)\dot{\boldsymbol{r}}_0 \tag{2.14b}$$

Solutions apart from the YA solution have been suggested for the TH equations. However, these can be proven to be equivalent to the YA solution excluding pathological and impractical cases. For example, Dang (2017) proves the equivalence of the Carter solution to the YA solution for $e \neq 1$. This condition holds for non-parabolic orbit and is hence applicable to our problem.

2.4.3 A Comparison of the Solutions

In elliptic orbits, the approximation of being circular holds only for a few kilometers around the target, with this radius decreasing with increasing eccentricity of the actual orbit. Depicted in Fig. 2.4 is the motion of a spacecraft that intends to reach the origin (location of the target) while following two trajectories, the red one based on the Yamanaka-Ankersen (YA) equations and the blue one based on the CWH equations for an orbit with eccentricity of 0.02 and computed as per the YA solution (all distance units are in km).

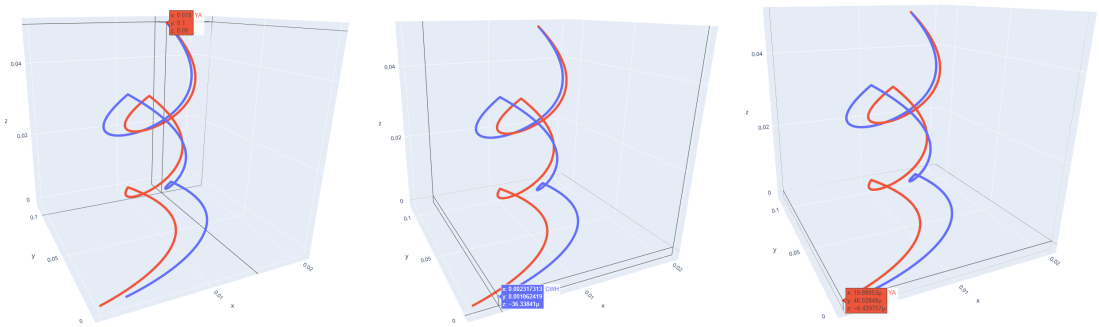

Figure 2.4: CWH solution vs YA solution in Elliptic Orbit

As is visible from the figure, the endpoint of the latter trajectory is off by a distance of 2.55 m from the origin, calling for the use of the elliptic orbit model for our application wherein spacecraft are required to perform close-distance operations and eventually docking.
Duzzi et al. (2016) suggest several simplifying conditions to reduce the complexity of the spacecraft formation problem. These include the following:

1. The target and the chaser are on the same orbital plane xz, and the relative motion is limited to this plane.
2. The satellite's attitude does not influence the thrusters' performance.
3. The distance between target and chaser is negligible with respect to the orbit radius.
4. The target is placed in the origin of the reference system.

However, these are considered for the circular orbit. In the generalization towards elliptic orbits, we strictly follow the second and fourth simplifications, and we follow the third condition to some extent. However, the YA solution does not restrict relative motion to a single plane.

2.5 Conversion of True Anomaly to Time and vice versa

The true anomaly of a spacecraft defines the position of the spacecraft moving along a Keplerian orbit. As suggested earlier, the YA solution and other solutions that base on the Tschauner-Hempel equations demand the representation of the state of the spacecraft in terms of the true anomaly. Although an actual spacecraft may have the required equipment to calculate an accurate reading for its true anomaly, it is imperative that we convert this parameter to time due to the required coherence of this step with the rest of the assembly problem.

There is no closed-form finite-polynomial solution for the value of true anomaly f that corresponds to time t after reaching the perigee. Hence, despite the accuracy attained in opting for the YA solution (elliptic orbit) instead of the CWH equations (circular orbit), we are constrained to approximate the value true anomaly in terms of time. We have the following relations between time t, mean anomaly M, eccentric anomaly E, and true anomaly f (Roy (2004)):

$$M = nt \tag{2.15}$$

$$M = E - e\sin E \tag{2.16}$$

$$\tan\frac{\theta}{2} = \sqrt{\frac{1+e}{1-e}}\tan\frac{E}{2} \tag{2.17}$$

From these, we obtain the approximation of f in terms of t (or M) up to the third place as:

$$f = nt + c_1\sin(nt) + c_2\sin(2nt) + c_3\sin(3nt) \tag{2.18a}$$

$$= M + c_1\sin(M) + c_2\sin(2M) + c_3\sin(3M) \tag{2.18b}$$

where $c_1 = 2e - \frac{e^3}{4}$, $c_2 = \frac{5}{4}e^2$, and $c_3 = \frac{13}{12}e^3$. This value of f may be fed into the YA solution to obtain the state transition matrix of the spacecraft with time being the independent variable.

2.6 Summary

Following a basic design of each spacecraft that we consider throughout this research, the chapter deals with an overview of orbital motion for a spacecraft in an elliptic orbit. In particular, we delve into the motion of a spacecraft with respect to the local-vertical-local-horizontal (LVLH) frame of reference, defined by the Euler-Hill equations, for both circular orbits (CWH equations) and elliptic orbits (TH equations). We adopt the Yamanaka-Ankersen solution for the case of elliptic orbits. Finally, we investigate the conversion between real time and true anomaly due to the dependence of the YA solution on the true anomaly of the central spacecraft.

Chapter 3

Positional Convergence and Collision Avoidance

3.1 Introduction

The spacecraft formation problem requires multiple spacecraft to converge at a predefined point or a predefined set of points from the point of deployment by the rocket. These points are defined with respect to the LVLH frame of the central spacecraft since the telescope is built around the central spacecraft. As a result, each spacecraft requires to propel itself according to the Tshauner-Hempel equations as described in Chapter 2. In effect, this can be developed for each spacecraft as a rendezvous problem to a particular point. This chapter looks into a commonly used guidance strategy for reaching a target in the LVLH frame. Moreover, it presents a comparison of three algorithms to study how multiple spacecraft can reach their target locations while incorporating collision avoidance and resource optimization.

3.2 Rendezvous Algorithms

A spacecraft (here, chaser spacecraft) following the CWH or TH equations tends to follow a non-linear path from its starting position to the final position in the LVLH frame of the central spacecraft (also, target spacecraft). While this may pose no issues to the positional convergence of the spacecraft, it may lead to issues in communication and sensing due to the varying orientation of the line of sight from the chaser to the target. We look into a rendezvous algorithm where this is incorporated and another algorithm that resolves the problems that arise subsequently.

3.2.1 Two-Impulse Rendezvous

The classical two-impulse rendezvous algorithm propels the spacecraft directly towards the final position without considering the requirement for line of sight. As a result, the spacecraft takes a curvilinear path from the start point to the end point. Its velocity at the start point is varied by applying a particular value of delta-v[1] obtained from the TH equations as follows.
Consider the start position at time $t = 0$ to be $\boldsymbol{r}_0$ and the start velocity before the application of velocity change to be $\dot{\boldsymbol{r}}_0^-$. The velocity $\dot{\boldsymbol{r}}_0^+$ required at $\boldsymbol{r}_0$ to arrive at the final position $\boldsymbol{r}_1$ in time T is obtained as (Hablani et al. (2002)):

$$\dot{\boldsymbol{r}}_0^+ = \Phi_{r\dot{r}}^{-1}(T)\left(\boldsymbol{r}_1 - \Phi_{rr}(T)\boldsymbol{r}_0\right) \tag{3.1}$$

where the matrices $\Phi_{rr}(t)$ and $\Phi_{r\dot{r}}(t)$ are obtained from the YA solution as explained in 2. From this relation, the required delta-v is computed as:

$$\Delta \boldsymbol{V}_0 = \dot{\boldsymbol{r}}_0^+ - \dot{\boldsymbol{r}}_0^- \tag{3.2}$$

The arrival velocity at $\boldsymbol{r}_1(T)$, denoted as $\dot{\boldsymbol{r}}_1(T)$, is given as:

$$\dot{\boldsymbol{r}}_1(T) = \Phi_{\dot{r}r}(T)\boldsymbol{r}_0 + \Phi_{\dot{r}\dot{r}}(T)\dot{\boldsymbol{r}}_0^+ \tag{3.3}$$

[1] change in velocity: a measure of the impulse per unit of spacecraft mass that is needed to perform a maneuver

which is countered by a delta-v at the final position as:

$$\Delta \boldsymbol{V}_1(T) = -\dot{\boldsymbol{r}}_1(T) \tag{3.4}$$

The two-impulse rendezvous algorithm, as described earlier, does not suit the needs of an actual spacecraft mission due to which we investigate the glideslope algorithm.

3.2.2 Multipulse Glideslope Rendezvous

A glideslope is a straight path from the current location of the chaser spacecraft to its intended destination, which may be a target spacecraft center of mass, a docking port, or a location of interest in space near a target. Hablani et al. (2002) develop the multipulse glideslope transfer wherein an inbound glideslope guidance is invoked when a chaser vehicle is required to approach a target vehicle. Thruster activity near the target location is to be minimized to avoid plume impingement on neighboring spacecraft and contamination of their surfaces. In addition, as a chaser approaches the target position, its relative velocity must diminish to certain safe limits. These requirements are fulfilled by designing a guidance trajectory wherein the range rate is proportional to the range.

Traveling on the glideslope for every instant requires continuous thrust which is not a practical option for spacecraft. Instead, the spacecraft makes jumps (in the LVLH frame) from one point on the glideslope to the next. In the LVLH frame, let the chaser be located at $\boldsymbol{r}_0$ with velocity $\dot{\boldsymbol{r}}_0^-$ and be required to arrive at $\boldsymbol{r} = \boldsymbol{r}_T$ in time T. The glideslope is a straight line from $\boldsymbol{r}_0$ to $\boldsymbol{r}_T$, denoted by $\boldsymbol{\rho}_0 = \boldsymbol{r}_T - \boldsymbol{r}_0$. Since the spacecraft is required to reach $\boldsymbol{r}_T$ at time T, $\boldsymbol{\rho}_T = 0$, and at time t, $\boldsymbol{\rho}(t) = \boldsymbol{r}(t) - \boldsymbol{r}_0$. This vector $\boldsymbol{\rho}$ can be represented in terms of the scalar distance ρ along the unit vector $\boldsymbol{u}_\rho$ as $\boldsymbol{\rho} = \rho \boldsymbol{u}_\rho$. As the distance-to-go ρ decreases, the speed of the spacecraft $\dot{\rho} = a\rho + \dot{\rho}_T$ must decrease as mentioned earlier, where $\dot{\rho}_0$ is predefined depending on the accuracy of the rendezvous operation, and a and $\dot{\rho}_T$ are computed as (Hablani et al. (2002)):

$$a = \frac{\ln \frac{\dot{\rho}_T}{\dot{\rho}_0}}{T} = \frac{\dot{\rho}_0 - \dot{\rho}_T}{\rho_0} < 0 \tag{3.5}$$

A desirable feature that arises as a side-effect is the decrease in the acceleration of the spacecraft $\ddot{\rho} = a\dot{\rho}$ due to the decrease in $|\dot{\rho}|$. Now we know that,

$$\text{At } t = 0: \quad \rho = \rho_0, \quad \dot{\rho} = \dot{\rho}_0 < 0 \tag{3.6a}$$

$$\text{At } t = T: \quad \rho = 0, \quad \dot{\rho} = \dot{\rho}_T < 0 \tag{3.6b}$$

With these boundary conditions, we obtain the general equation for ρ as:

$$\rho(t) = \rho_0 e^{at} + \frac{\dot{\rho}_T}{a}(e^{at} - 1) \tag{3.7}$$

Now, consider the number of thruster firings to travel from $\boldsymbol{r}_0$ to $\boldsymbol{r}_T$ in time T to be N and the uniform interval between any two successive pulses to be $\Delta t = T/N$; i.e. thrusters are fired at $t_m = m\Delta t$, $m = 0, 1, ..., N-1$. The mth pulse pushes the chaser from $\boldsymbol{r}_m$ to $\boldsymbol{r}_{m+1}$ where:

$$\boldsymbol{r}_m = \boldsymbol{r}_T + \rho_m \boldsymbol{u}_\rho \tag{3.8}$$

$$\rho_m = \rho(t_m) = \rho_0 e^{at_m} + \frac{\dot{\rho}_T}{a}(e^{at_m} - 1) \tag{3.9}$$

Subsequently, the algorithm operates based on the same principle of the two-impulse rendezvous algorithm by jumping from one intermediate (at first, start) point to the next intermediate (finally, end) point. The applied delta-v at each intermediate point does not bring the spacecraft to a stop but rather pushes it onto the next point.

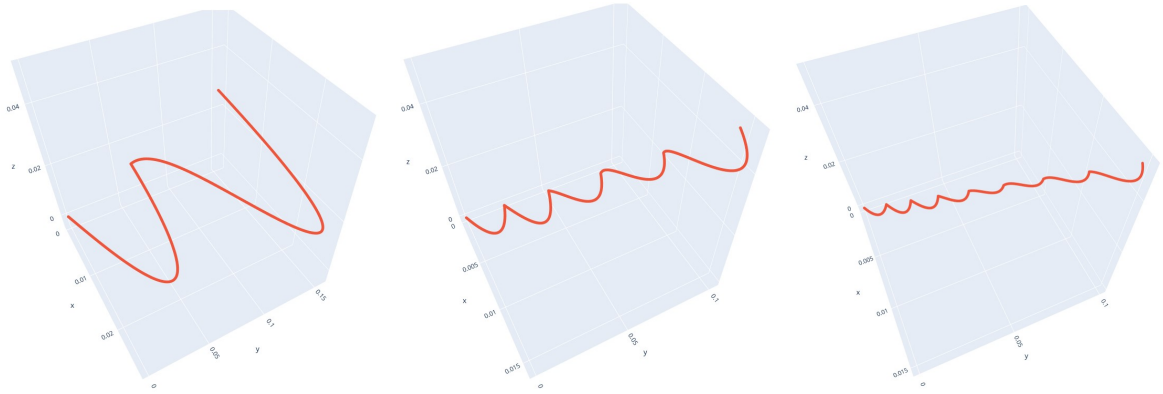

(a) 2 Steps (b) 5 Steps (c) 8 Steps

Figure 3.1: Basic Glideslope Algorithm

The glideslope algorithm, as observed in an elliptic orbit, is represented in Fig. 3.1 with the number of steps at 2, 5, and 8. The significant improvement in following the line of sight with increasing the number of steps is visible from the figures.

3.3 Optimization Algorithms

In the presence of multiple spacecraft converging at nearby positions, it is very probable for collisions to occur. Moreover, the possibility for each spacecraft to reach any one among a set of multiple positions allows the system to minimize resources consumed by all spacecraft by optimizing the allocation of target locations to each spacecraft. We specifically consider the minimization of distance for this purpose and investigate the effectiveness of three distributed algorithms that are run on all the spacecraft on reaching each intermediate point in the glideslope algorithm. In an actual scenario, with sufficient computational power, this may also occur throughout the course of the jump.

3.3.1 Distributed Greedy (Handshake) Algorithm

We develop a greedy algorithm wherein each spacecraft performs a myopic algorithm as explained in Algorithm 1. Here, $intNeighbors$ is a list of $numAgents$ lists where the ith list enumerates the neighbors of agent i with intersecting lines and $intersecting$ is a list of $numAgents$ booleans where the ith boolean represents if agent i has any intersection. Each spacecraft checks for intersections of the line of sight to its target location and such lines of its neighbors. The target locations are exchanged for each intersection such that the intersection is resolved. This process is continued for the spacecraft until all intersections are resolved.

Let us consider the variation in the total length of the unsolved configuration due to such exchanges. Since the sum of two sides of a triangle is larger than the third side, it can be deduced that solving each intersection reduces the total length of the configuration. If the total length of the configuration cannot be decreased, it certainly does not contain an intersection because solving the intersection will decrease the total length which is a contradiction. Hence, the configuration with least total length is a solution to the problem. However, there may also exist other sub-optimal solutions that do not contain intersections. The greedy algorithm will terminate as soon as it reaches any such solution. Hence, it may not provide the shortest possible

total line-of-sight distance for the configuration but it will prevent the occurrence of collisions. The implementation of the algorithm is depicted in Fig. 3.2a.

Algorithm 1: Distributed Greedy (Handshake) Algorithm

Result: Positional Convergence

```
while True do
    Compute intNeighbors and intersecting
    if all (intersecting) = False then
        Algorithm is complete. Break the loop.
    end
    forall agent ∈ {1,2,...,numAgents} do
        if intersecting[agent] then
            forall neighbor ∈ intNeighbors[agent] do
                Exchange target locations of agent and neighbor
                Recompute intersecting[agent], intNeighbors[agent]
                if not (intersecting[agent]) then
                    Break inner loop
                end
            end
        end
    end
end
```

3.3.2 Zavlanos-Spesivtsev-Pappas (ZSP) Auction Algorithm

Zavlanos et al. (2008) propose a solution to the assignment problem based on the auction algorithm that was developed by Bertsekas (1979) and Bertsekas and Castañon (1991), wherein only local information is available to each agent. This algorithm always converge to an assignment that maximizes the total reward within a linear approximation of the optimal one.

Algorithm 2: Zavlanos-Spesivtsev-Pappas Auction Algorithm (Zavlanos et al. (2008))

Result: Positional Convergence

if *Graph* $\mathscr{G}$ *is not connected* **then**

Algorithm cannot be performed.

Return initial target allocation

end

a: a list of *numAgents* integers, all initialized to 0

b: a list of *numAgents* lists of *numAgents* floating point numbers, all initialized to 0

p: a list of *numAgents* lists of *numAgents* floating point numbers, all initialized to 0

while $a(t+1)$ *contains repetitions* **do**

forall $i \in$ *{1,2,...,numAgents}* **do**

forall $j \in$ *{1,2,...,numAgents}* **do**

$p_{i,j}(t+1) = \max(p_{k,j}(t) \forall k \in \mathscr{N}_i \cup \{i\})$

$b_{i,j}(t+1) = \max(b_{k,j}(t) \forall k \in argmax_{z \in \mathscr{N}_i \cup \{i\}}(p_{z,j}(t)))$

end

if $p_{i,a_i(t)}(t) \leq p_{i,a_i(t+1)}(t)$ *and* $b_{i,a_i(t)}(t+1) \neq i$ **then**

$a_i(t+1) = argmax_{1 \leq k \leq m}\{\beta_{ik} - p_{i,k}(t+1)\}$

$b_{i,a_i(t+1)} = i$

$v_i = max([beta_{i,k} - p_{i,k}(t) \forall k \in range(numAgents)])$

$w_i = max([beta_{i,k} - p_{i,k}(t) \forall k \in range(numAgents), k \neq a_i(t+1)])$

Assign random value to ε

$\gamma_i = v_i - w_i + \varepsilon$

$p_{i,a_i(t+1)}(t+1) = p_{i,a_i(t+1)}(t) + \gamma_i$

end

end

Update $a(t)$, $b(t)$, $p(t)$ with $a(t+1)$, $b(t+1)$, $p(t+1)$

end

Given in Algorithm 2 is the implementation of the ZSP algorithm over all agents for a single allocation problem. This is repeated at each intermediate point of the glideslope trajectory to compute the optimal target allocation for the agents. In the given algorithm, β is a constant list of *numAgents* lists of *numAgents* floating point numbers where the jth number of the ith list denotes the cost of reaching target j by agent i, a is a list of *numAgents* integers where the ith number represents the target assignment of agent i, b is a list of *numAgents* lists of *numAgents*

floating point numbers where the jth number of the ith list denotes the largest-index bidder among the possibly multiple highest bidders for target j, and p is a list of $numAgents$ lists of $numAgents$ floating point numbers where the jth number of the ith list denotes the price of allocating target j to agent i.

As observed in Fig. 3.2b, the algorithm provides an optimal trajectory such that the cumulative length of the lines of sight of the spacecraft is at the minimum attainable value. This ensures, through the logic explained in the description of the distributed greedy algorithm, that collisions are avoided among the spacecraft.

3.3.3 Distributed Hungarian Algorithm

The assignment problem refers to the problem of allocating N tasks among N agents with each allocation incurring a cost that may vary depending on the agent and the task such that the total cost of all allocations is minimized. In their historical paper on the Hungarian algorithm for the assignment problem, Kuhn and Yaw (1955) solve this problem in polynomial time by adjusting the incurred cost for each agent-task allocation and find the suitable lowest costs over specific intervals. This has further been developed into a graph theoretical setting by Kuhn (1956).

We adopt this algorithm as what we describe the 'Distributed Hungarian Algorithm', into the positional convergence problem such that each spacecraft performs a version of the Hungarian algorithm such that an optimal arrangement of final positions is obtained at each spacecraft for itself and its neighboring spacecraft. Such an algorithm will provide the same output as the ZSP algorithm if both follow identical patterns of communication. Instead, in order to emulate the absence of multiple communications among spacecraft for faster convergence to the result, we consider this algorithm without the presence of feedback from neighboring spacecraft; i.e., each spacecraft performs the Hungarian algorithm locally and approaches the hence computed target location while the local computation of one spacecraft is not affected by the simultaneous local computation of a neighbor.

While such a mechanism can be advantageous in terms of computational speed, it is highly disadvantageous due to the possibility of multiple spacecraft approaching the same intermediate/final point or not resolving possible collisions and resulting in imminent impact. Moreover, This can be observed in Fig. 3.2c.

3.3.4 A Comparison of the Algorithms

We compare the three algorithms using three test cases, each of which considers randomly generated start points while having the same end points corresponding to the unorganized pre-assembly stage of the space telescope. The outputs of the three algorithms are generated for three levels of communication capability:

- high communication capability: the graph is connected from the start point,
- medium communication capability: the graph is connected from some intermediate point but before the spacecraft are in close physical proximity with each other,
- low communication capability: the graph is connected from some intermediate point close to the end point

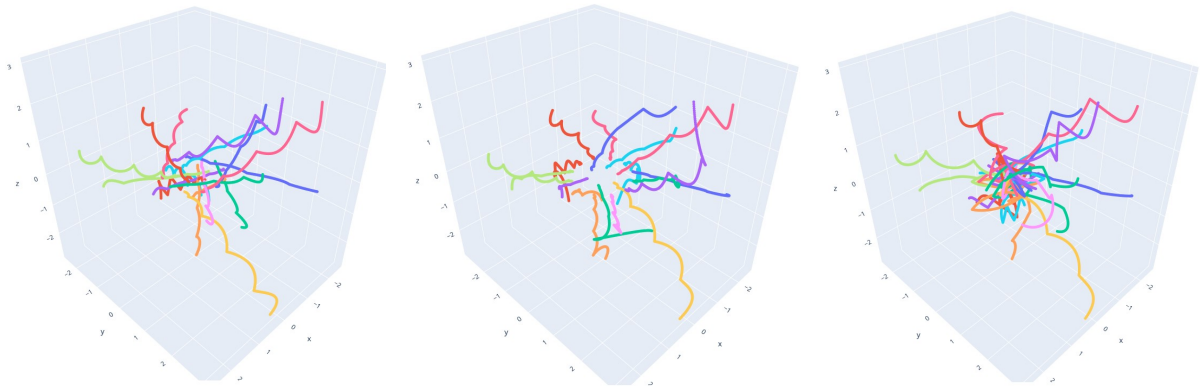

(a) Distributed Greedy Alg. (b) ZSP Auction Algorithm (c) Distributed Hungarian Alg.

Figure 3.2: Achieving Unorganized Pre-assembly using three different algorithms

While Fig. 3.2 provides a comparison between these algorithms in a particular test case with high communication capability, the corresponding figures for all these test cases are provided in Appendix A. As observed from these cases, the ZSP Auction Algorithm, though requiring the graph to be complete, solves the allocation problem for the entire graph at once. As a result, the total distance traveled by all spacecraft is optimized although each spacecraft may not be assigned to its nearest target location. This is in compliance to the nature of the general auction algorithm.

The Greedy Algorithm does not require the completeness of the communication graph. However, it is effective only for close approaches or collisions between spacecraft and hence seldom

exchanges the target locations. This subsequently reduces the arbitrariness in its decisions.
The results of the Distributed Hungarian Algorithm are not satisfactory although it does not require graph completeness. Though attempting to solve the minimum-sum-of-distances problem similar to the ZSP Algorithm, the level of localization is higher and the spacecraft enacts based on its auction prior to receiving feedback from its neighbors; i.e. there is only a single iteration of determining the final location for each jump. As a result, this algorithm may also lead to collisions since the information stored by one spacecraft may clash with the information stored by its neighbors. In essence, the algorithm behaves as a 'Feedback-less Algorithm'.

From the above algorithms, it can be understood that either the Greedy Algorithm or the ZSP Algorithm may be implemented for the construction of the space telescope. A hybrid may also be implemented, wherein the former algorithm is used to prevent collisions with neighbors until the graph is complete and the latter algorithm is used thereafter to optimize the trajectory of all spacecraft. There are several other implementations of the auction algorithm that suit the above problem. One such example is the Consensus-Based Auction Algorithm (CBAA) as proposed by Choi et al. (2009) (adopted in Lusk et al. (2020)) that deals with task allocation using consensus techniques for each agent to communicate details of the assignment to neighbors. However, it may be deduced that all such algorithms result in identical or almost-identical solutions, all of which avoid collisions and optimize the trajectory of all spacecraft. Hence, the choice of distributed auction algorithm is up to the discretion of the mission planner.

3.4 Summary

This chapter deals with two different types of algorithms: rendezvous algorithms and optimization algorithms. The multipulse glideslope rendezvous algorithm (Hablani et al. (2002)) is discussed in comparison to the two-impulse rendezvous algorithm, and is observed to follow the line of sight to the central spacecraft much more religiously than the latter technique.
Among optimization algorithms, we look into the Zavlanos-Spesivtsev-Pappas (ZSP) Distributed Auction Algorithm. We also design two algorithms: the Distributed Greedy (Handshake) Algorithm, based on greedy exchanges of target locations, and the Distributed Hungarian Algorithm, based on the distributed implementation of the Hungarian algorithm. Despite its capability of providing the optimal assignment when centralized, the latter performs worst among the three

due to the lack of feedback from neighbors. Considering the ZSP algorithm and the greedy algorithm, we have seen that the former provides more optimal results since it minimizes the total distance (a consequence of the assignment problem). However, the latter is much simpler in design and it functions even in the lack of a complete graph, due to which an actual spacecraft formation system may adopt a hybrid of the two algorithms to perform positional convergence.

Chapter 4

Off-Axis Paraboloidal Mirrors and Configuration Rearrangement

4.1 Introduction

Due to the property of focusing energy at a defined point called the *focus*, paraboloidal reflectors are very often used to collect energy from a distant source. As reflecting telescopes, such paraboloidal mirrors with predefined characteristics have been built across the planet as well as deployed to space to gather light (across the spectrum) from galaxies, stars, and star systems. Telescopes in orbit prove much more effective than those on the earth since they avoid a decrease in their resolving power due to the lack of atmospheric fluctuations. However, it is not possible to deploy extremely large telescopes to space with the structural and propulsive technology that exists today. This chapter provides general details on paraboloidal mirrors and delves specifically into the parameterization of off-axis paraboloidal mirrors which, when mounted together, form a single large paraboloidal mirror. In particular, we look into the formulation of almost-exact target locations for each spacecraft. We investigate why the optimization algorithms proposed in Section 3.3 are insufficient to acquire the final configuration

of the telescope and we develop an algorithm with collision avoidance to resolve this problem.

4.2 Properties of Paraboloidal Mirrors

According to McLean (2008), all large astronomical telescopes today, from the ultraviolet range to radio range, are reflectors and use curved mirrors for light collection and focusing. However, using spherical-shaped mirrors, as initially used by Newton, results in spherical aberration unless the focal length is very long, i.e., parallel incident rays at increasing lateral heights cross the axis closer and closer to the mirror. A conic section will solve this problem. Conic sections are so-named since they are all derived from cross-sectional cut through a cone. A fundamental property of a conic section shape is that any ray starting at one focus will form a perfect point image at the other. For a parabola, one focus is at infinity, and therefore rays from that focus are parallel to the axis and all such rays meet at the other focus.

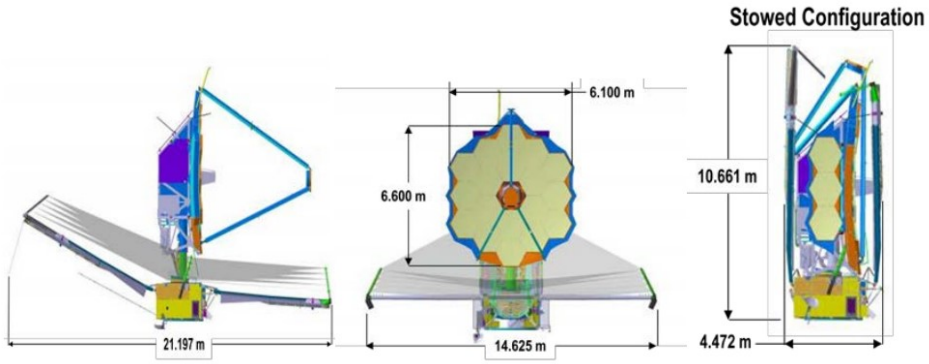

Figure 4.1: James Webb Space Telescope (Greenhouse (2019))

The motivation for building larger ground-based telescopes has been clear for a very long time: for a telescope of fixed resolution, the observing time necessary to reach a given signal-to-noise ratio varies as $1/D^2$, where D is the diameter of the primary mirror. However, building a giant telescope from a single monolithic mirror presents many difficulties that typically grow rapidly with increasing mirror size and make building such mirrors with diameters of 10 m or more highly impractical. According to Oswalt and McLean (2013), constructing the primary mirror of a telescope out of segments, rather than from a monolithic piece of glass, can drastically reduce the mass of the mirror and its material costs, thereby making possible the construction of telescopes with very large diameters. Segmentation has also made possible space telescopes such as the 6.5-m James Webb Space Telescope, that is set to launch in October 2021.

4.3 Segmentation Geometry

According to Bely (2003), segmentation can be performed as two geometries: 'petals'/'keystones' and 'hexagons'. The 'petals' geometry uses segments that are slices in radial and azimuthal coordinates while the 'hexagons' geometry uses segments of nearly identical-sized hexagons as depicted in Fig. 4.2. While petals have the advantage of adopting a circular periphery, hexagons require only a single support type; i.e., all spacecraft may adopt the same design irrespective of location.

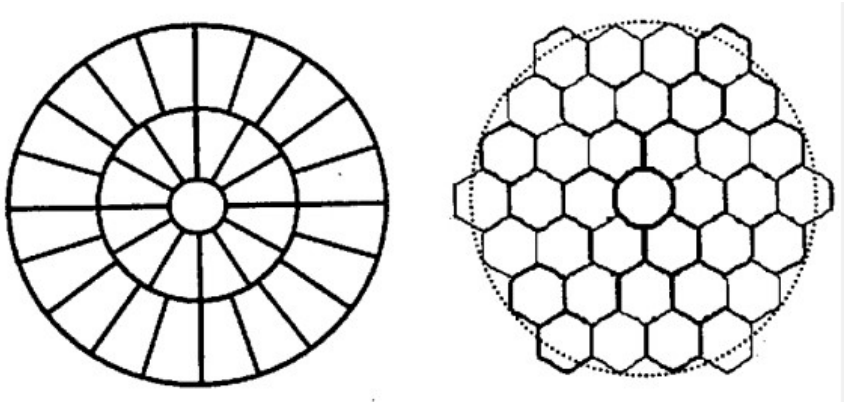

Figure 4.2: 'Petals' and 'Hexagons' Geometries (Bely (2003))

The hexagonal geometry is built up as 'layers' (or 'rings') without a central segment or a segment with a hole in its center. With no central segment, the total number of segments N_{agents} is given as a function of the number of layers N_{layers} (Bely (2003)):

$$N_{agents} = 3N_{layers}\left(N_{layers}+1\right) \tag{4.1}$$

Here, the lth layer, considering the central spacecraft to be layer 0, contains $6l$ segments.

4.4 Parameterization of Off-Axis Paraboloidal Mirrors

Segmented paraboloidal mirrors end up being the imprint of a particular shape, mostly hexagonal, on a separated segment of a paraboloidal mirror which is referred to as an *off-axis paraboloidal mirror*. Based on information procured from the NASA James Webb Space Telescope group, the primary mirror segments are sections of a paraboloid, so each hexagonal shaped mirror is

an off axis paraboloid which have been cookie cut from the larger parabola.

Despite the advantages of OAP mirrors due to which they are used to construct large telescopes, one of the main practical challenges faced in building an optical system including OAPs is the unclear or poorly defined datum or geometry parameters that associate with such mirrors. Han et al. (2019) provide systematically organized information on the geometrical properties of off-axis paraboloidal mirror segments.

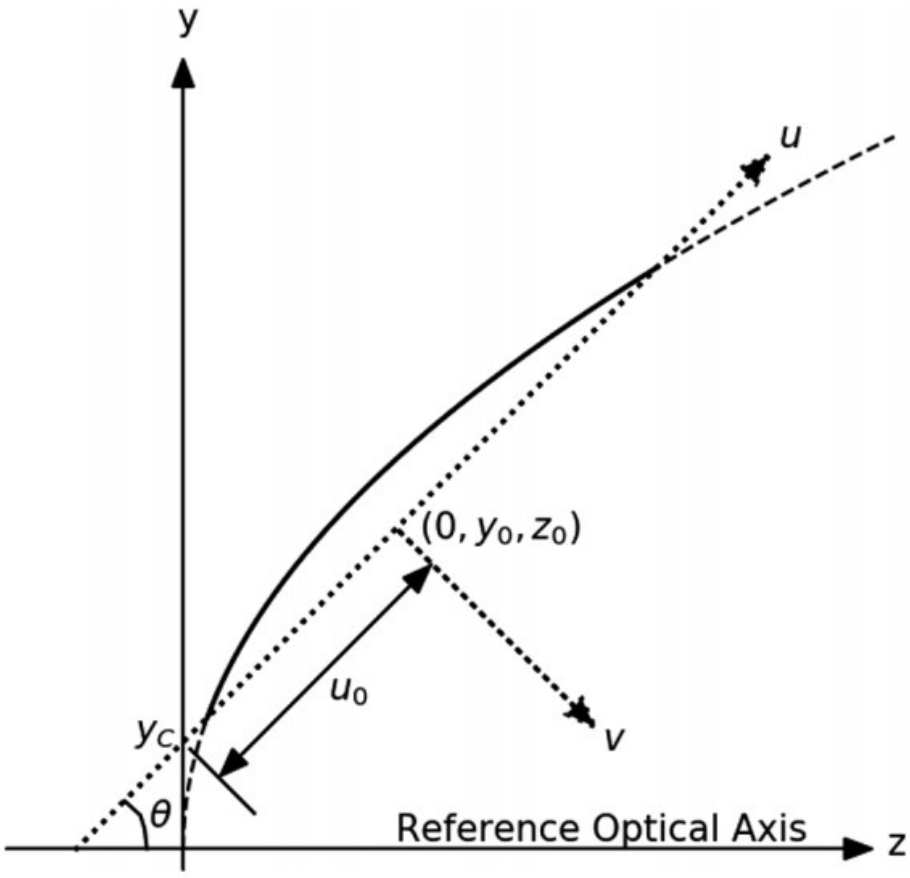

Figure 4.3: Parabolic surface (Han et al. (2019))

Consider a section of a paraboloid as depicted in Fig. 4.3 where the z axis and origin coincide with the ROA and vertex of the paraboloid, respectively. For R being the radius of curvature of the paraboloid, the sink of the paraboloid can be expressed as (Han et al. (2019)):

$$z(x,y) = \frac{x^2+y^2}{2R} \tag{4.2}$$

$$\text{or, } x^2+y^2 = 2Rz \tag{4.3}$$

The dotted straight line represents a plane that intersects with the xy plane of the system at

$y = y_C$ with an angle θ to the xz-plane. The plane, called the *aperture plane*, also intersects with the paraboloid and the section that it cuts out represents the required OAP.

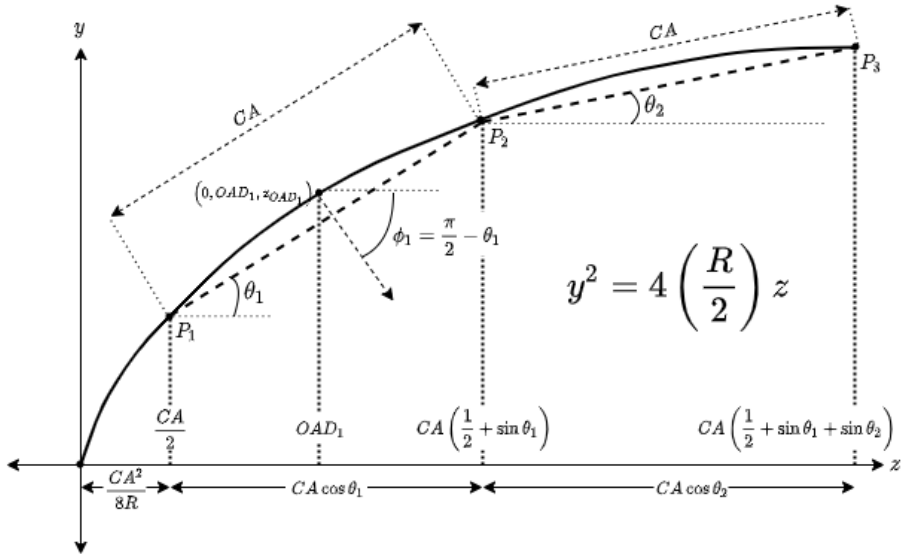

Figure 4.4: Parabolic surface with Position and Orientation of Spacecraft

We assume that all segments of the mirror have equal clear apertures[1] (CA). Considering the origin of the above plot to coincide with the center of mass of the central spacecraft, each OAP mirror should be attached to its carrying spacecraft at the points $(0, \mathrm{OAD}_i, z_{\mathrm{OAD}_i})$ [2]. Here, the off-axis distance (OAD) is the vertical distance from the reference optical axis to the aperture center which we assume identical to the center of mass. The point $(\mathrm{OAD}_i, z_{\mathrm{OAD}_i})$, while satisfying the parabola equation $y^2 = 4\left(\frac{R}{2}\right)z$, also lies on a tangent whose slope is the tangent of the angle θ_i. This tangent, from the standard relations of a parabola, can be written as:

$$y = \frac{2\frac{R}{2}}{\mathrm{OAD}_i} z + \frac{2\frac{R}{2}}{\mathrm{OAD}_i} z_{\mathrm{OAD}_i} \tag{4.4}$$

Hence, the following relations can be developed between the angle θ_i, OAD_i, and z_{OAD_i}:

$$\tan\theta_i = \frac{2\frac{R}{2}}{\mathrm{OAD}_i} \implies \mathrm{OAD}_i = \frac{R}{\tan\theta_i} \tag{4.5}$$

$$z_{\mathrm{OAD}_i} = \frac{\mathrm{OAD}_i^2}{2R} = \frac{R}{2\tan^2\theta_i} \tag{4.6}$$

[1] the diameter or size of an optical component that must meet specifications

[2] the x coordinate will be ignored hereafter

With the central spacecraft having a pitch of the spacecraft needs to have an effective pitch $\phi_i = \frac{\pi}{2} - \theta_i$ that depends on the final layer of the spacecraft. In order to compute ϕ_i, we define the point P_l as the boundary points of the corresponding OAP mirrors, where l is the larger layer number of the two neighboring mirrors. These points can be represented with the following relations:

$$P_1 \equiv \left(\frac{\mathrm{CA}}{2}, \frac{\mathrm{CA}^2}{8R}\right) \tag{4.7}$$

$$P_{l+1} \equiv \left(\mathrm{CA}\left(\frac{1}{2} + \sum_{i=1}^{l} \sin\theta_i\right), \mathrm{CA}\left(\frac{\mathrm{CA}}{8R} + \sum_{i=1}^{l} \cos\theta_i\right)\right) \tag{4.8}$$

However, these points also satisfy the parabola equation:

$$P_{l+1}[z] = \frac{P_{l+1}[y]^2}{2R} \tag{4.9}$$

Provided the radius of curvature R and the clear aperture CA of the parabola, the above relations can be used to solve for the value of θ_i iteratively.

The above computation has been performed for a single segment (dark orange segment 0 in Fig. 4.5) on the lth (or $l+1$th) layer of a parabolic mirror where this segment lies on the $x = 0$ axis. However, there are other segments (yellow segments in Fig. 4.5) which, together with this segment, will form the entire layer. The z coordinates of the cm of these segments remain equal to that of segment 0. However, their x and y coordinates vary such that they lie equidistant from the cm of the central spacecraft and their neighbors. Let the y coordinate of segment 0 be renamed as $P_{l+1,0}[y]$ and $N_{agents(l+1)}$ be the number of spacecraft in the layer. Then, the x and y coordinates of segment i are given as:

$$P_{l+1,i}[x] = P_{l+1,0}[y] \times \sin\left(\frac{2\pi i}{N_{agents(l+1)}}\right) \tag{4.10a}$$

$$P_{l+1,i}[y] = P_{l+1,0}[y] \times \cos\left(\frac{2\pi i}{N_{agents(l+1)}}\right) \tag{4.10b}$$

The spacecraft of the non-‘0’ segments of the layer not only have different x and y coordinates but also different orientations. While the pitch of all spacecraft in a layer are equal and the roll of all spacecraft are zero irrespective of their layer number (as will be observed in Chapter 5), the yaw of each spacecraft in a layer will be indicative of its segment number. This will be

discussed in the next chapter.

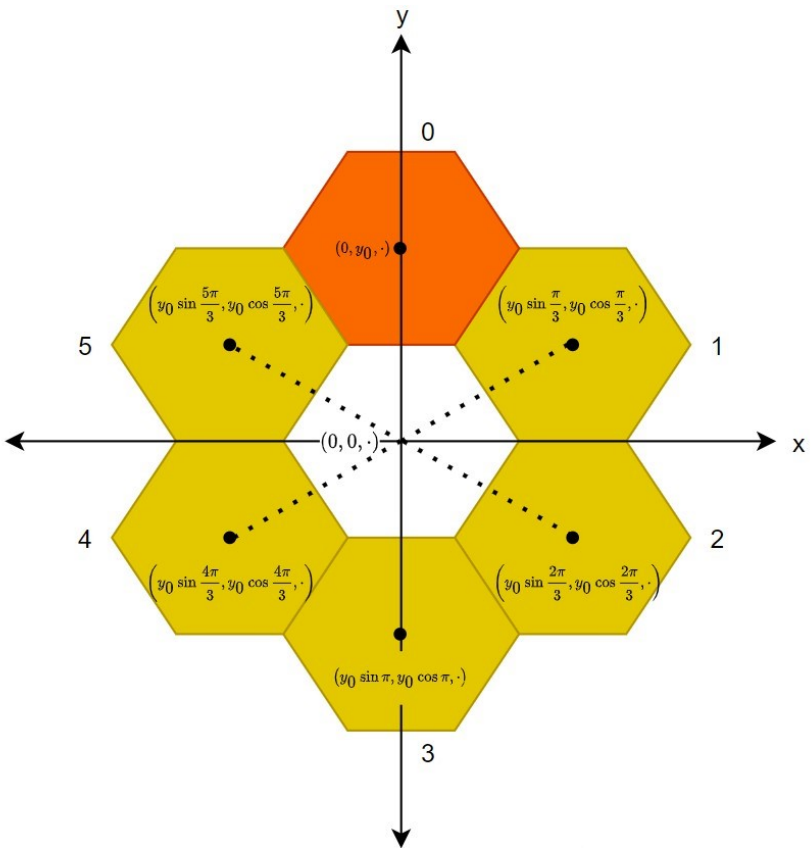

Figure 4.5: Single Layer Mirror Segments

4.5 Intra-Formation Mutual Exchange Algorithm (IFMEA)

OAP mirrors are non-uniform; i.e., an OAP chosen from an arbitrary location is identical in structure to another OAP only if they posses the same layer number. Here, the layer number of an OAP refers to the shortest number of OAPs that should be encountered while drawing a straight line from the center of the entire mirror to the center of the OAP mirror. As a result, spacecraft carrying the OAP mirrors cannot interchange each others' locations freely but only among those lying in the same layer.

An option that does not involve active control from the spacecraft is the use of space robot manipulators as suggested by She et al. (2020) that may behave as standalone units or connected to the central spacecraft. However, such actuators may cause serious damage to the delicate segments of the telescopes that are mounted on each spacecraft. Another option is to enact a heterogeneous auction algorithm as suggested by Foust et al. (2020). However, since the sizes

of the spacecraft are comparable to the distance between them, such a technique again poses high risk to the safety and integrity of the telescope segments. We propose that, following the positional convergence of the spacecraft to some unorganized pre-assembly configuration as suggested in Chapter 3, a simple exchange algorithm, the Intra-Formation Mutual Exchange Algorithm (IFMEA), be followed in a step-by-step manner as depicted in Fig. 4.6.

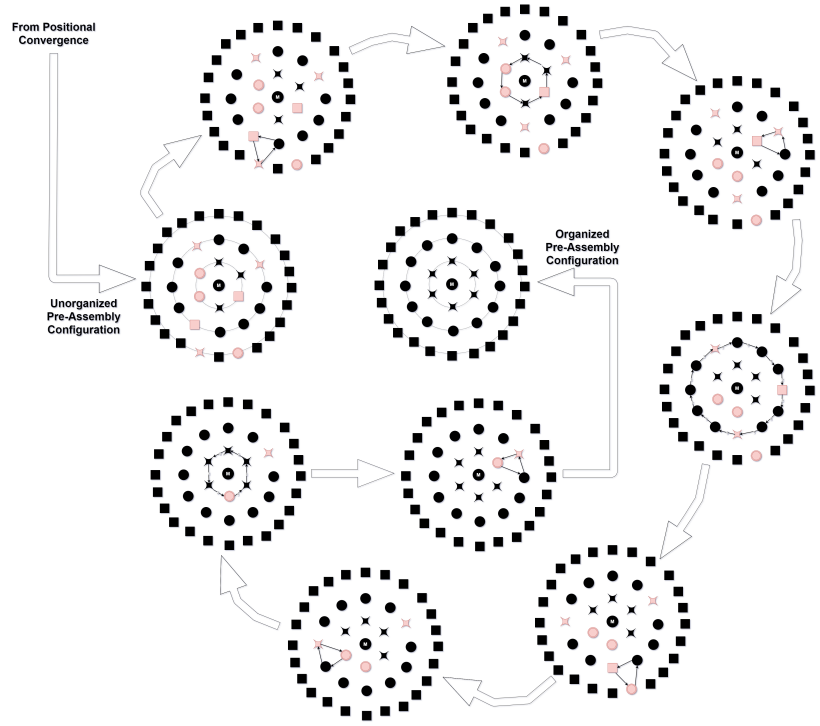

Figure 4.6: Basic Flowchart of IFMEA

In IFMEA, the central spacecraft searches for and iteratively solves the closest mismatch that can be solved using the smallest number of exchanges and with the minimum number of mismatches excluding the existing one (this is inherently guaranteed since the mismatch will be the closest possible in the entire formation). Let the layer number of the central spacecraft be 0. The algorithm is described in Alg. 3 where the keywords and functions are defined as follows:

- *maxN* represents the maximum layer number
- N is the layer number to which a spacecraft belongs by virtue of its predefined geometry
- L is the layer number to which a spacecraft belongs by virtue of its present position
- $S_{N,L}$ is a spacecraft presently on layer L that belongs to layer N by virtue of geometry
- $P_{L,i}$ is the configuration coordinate of a spacecraft on layer L and the value i represents its

present location with $i = 0$ being the spacecraft at $(0, \mathrm{OAD}_L, z_{\mathrm{OAD}_L})$

- the function $layer(T)$ provides the present layer number of a spacecraft T

Algorithm 3: Intra-Formation Mutual Exchange Algorithm

Result: Arranged Pre-assembly Configuration

$N \leftarrow maxN$;

while $N > 0$ **do**

  $L \leftarrow N - 1$;

  while $L > 0$ **do**

    while $num(S_{N,L}) > 0$ **do**

      Pick a spacecraft $S_{N,L}$ at some position $P_{L,i}$. Let us call this spacecraft T;

      while $layer(T) < N$ **do**

        1. Rotate the entire layer L in stages to bring T close to any mismatched spacecraft $U = S_{n,L+1}$ on layer $L+1$ and $n \neq L+1$. Consider V to be a neighbor of spacecraft U on layer $L+1$
        2. Perform the following exchange:
           - T $\rightarrow$ Location of V
           - V $\rightarrow$ Location of U
           - U $\rightarrow$ Location of T

      end

    end

    $L \leftarrow L - 1$

  end

  $N \leftarrow N - 1$

end

In the case of there being no mismatch on the layer $L+1$, the spacecraft $T = S_{N,L}$ is exchanged with any arbitrarily chosen spacecraft on the layer $L+1$. This creates a new mismatch which will be resolved when $N = L+1$. Although it is possible to simultaneously perform the algorithm for all spacecraft $S_{N,L}$, sequential application for each spacecraft ensures the convergence of the algorithm since a mismatched spacecraft from the outermost layer that is pushed inwards at some point will come to the outermost layer in its own turn. Performing this simultaneously for multiple spacecraft may cause mismatches and clashes in the rotations and exchanges.

The Intra-Formation Mutual Exchange Algorithm is performed for a telescope with two layers, the inner one with 6 segments and the outer one with 12 segments, hence emulating the struc-

ture of the James Webb Space Telescope. This is done following the positional convergence of the 18 spacecraft into the positions of the configuration in the LVLH frame of the central spacecraft. A snapshot of the positional convergence (using the ZSP auction algorithm) is presented in Fig. 4.7a and the subsequent use of IFMEA is provided in Fig. 4.7b. The synchronization of attitudes (step 3) for these spacecraft are represented in Fig. 5.2 in Chapter 5.

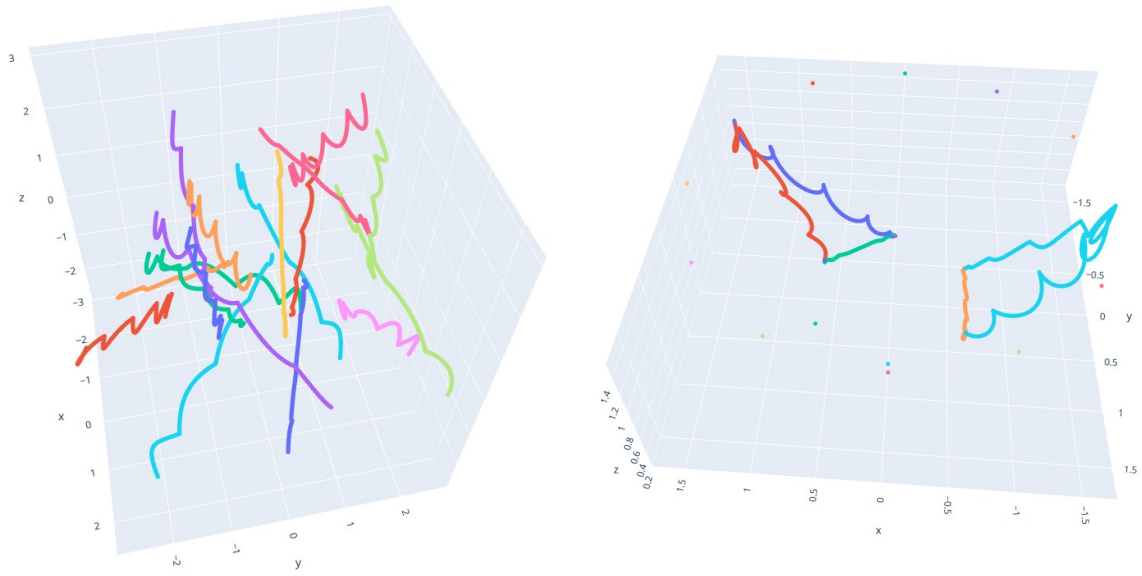

(a) Positional Convergence

(b) IFMEA

Figure 4.7: Steps 1 and 2: Spacecraft Formation using 18 spacecraft

This algorithm may be modified as per the structure of the telescope; i.e., depending on whether it follows a layer-based structure or not; but the essence of the algorithm is the iteration between the rotation of a particular cyclic group of spacecraft and the exchange of positions among three or more spacecraft such that collisions are avoided.

A possible issue with the algorithm is plume impingement that may be caused due to the close proximity of the spacecraft. This can be solved by suitably determining the space between the spacecraft for positional convergence; i.e. determining the multiple for the coordinate of each point; and moving them closer only after the attitude consensus stage that is dealt with later.

4.6 Summary

In this chapter, we have discussed the necessity of segmentation in paraboloidal mirrors and the reasons behind the choice of hexagonal segments over petal-life segments. We based our

analysis of off-axis paraboloidal mirrors, that are formed by the segmentation of paraboloidal mirrors, on the parameterization of such mirrors by Han et al. (2019) and we develop almost-exact positional parameters of each spacecraft based on the clear aperture of the segment and the radius of curvature of the paraboloid. The analysis depicts why each spacecraft is constrained to belong to a particular layer around the central spacecraft as a result of which we develop an exchange algorithm that moves each misplaced spacecraft to its actual layer while avoiding collisions. This algorithm can be further modified for other designs.

Chapter 5

Pre-Assembly Configuration-Based Attitude Consensus

5.1 Introduction

While the position of the spacecraft is determined using techniques that consider orbital parameters and mission requirements, attitude control is used to orient the spacecraft to facilitate docking with neighboring spacecraft. Our application, due to the close proximity of each spacecraft with several others, permits this operation to be performed using decentralized consensus. This chapter presents basic ideas from existing literature on multi-agent consensus with specific emphasis on attitude consensus. Furthermore, simulations are demonstrated in the time-variant framework at the pre-assembly stage of the spacecraft formation, and the corresponding results depict the convergence of individual attitudes to the expected value. The final attitude for each spacecraft is determined from its actual layer number and position in the layer at the time of measurement along similar lines as the calculation of the final position from the properties of off-axis paraboloidal mirrors in Chapter 4.

5.2 Attitude Dynamics and Kinematics

Reference coordinate systems change for a spacecraft depending on the task that it is involved in during the given period of its life. The orbit reference frame is one whose origin moves with the cm of the spacecraft and in which the spacecraft is three-axis attitude-stabilized[1]. The z-axis $\boldsymbol{Z_R}$ points toward the cm of the earth, $\boldsymbol{X_R}$ is in the direction of the velocity of the spacecraft in the plane of the orbit, and $\boldsymbol{Y_R}$ (normal to the plane of the orbit) completes a three-axis right-hand orthogonal system.

The attitude of a satellite can be defined with respect to a reference frame using a direction cosine matrix $[\mathbf{A}]$, a quaternion vector $\mathbf{q}$, or Euler angles. There are other representations that are used such as the classical and modified Rodriguez parameters, as explained by Terzakis et al. (2018), and the Cayley-Klein parameters (Goldstein et al. (2000)). Our research will investigate the attitude consensus problem in the Euler angles (more accurately, the Tait-Bryan angles) defined by the rotation sequence of z-y'-x" (intrinsic rotations) or x-y-z (extrinsic rotations), where the first rotation corresponds to 'yaw', ψ, the second to 'pitch', θ, and the third to 'roll' ϕ. These can be converted to a rotation matrix as:

$$A = A_Z A_Y A_X \tag{5.1}$$

where the individual matrices for the axes are given as:

$$A_X = \begin{bmatrix} 1 & 0 & 0 \\ 0 & \cos\phi & -\sin\phi \\ 0 & \sin\phi & \cos\phi \end{bmatrix} \tag{5.2a}$$

$$A_Y = \begin{bmatrix} \cos\theta & 0 & \sin\theta \\ 0 & 1 & 0 \\ -\sin\theta & 0 & \cos\theta \end{bmatrix} \tag{5.2b}$$

$$A_Z = \begin{bmatrix} \cos\psi & -\sin\psi & 0 \\ \sin\psi & \cos\psi & 0 \\ 0 & 0 & 1 \end{bmatrix} \tag{5.2c}$$

[1] the spacecraft is held fixed in the frame at a desired orientation without any rotation

This matrix A may further be suitably transformed into the other representations.

5.3 Multi-Agent Collective Control

A multi-agent system refers to a group of autonomous agents operating in a networked environment. While an individual system is controlled by its trajectory in the time dimension, denoted by $x(t)$ at time t, Knorn et al. (2016) represent a multi-agent system $M = (x_1(t,k)),(x_2(t,k))$ as a two-dimensional model with system behavior $x_1(t,k)$ and network influence $x_2(t,k)$ at time t and agent index k. $n(t,k)$ denotes the neighbors of agent k at time t, and $\tau(t,k)$ denotes the time of measuring this state. The system dynamics of the system M is analyzed in the time domain:

$$\delta x_1(t,k) = f(x_1(t,k), x_2(t,k), t, k) \tag{5.3}$$

where δx_1 represents the continuous or discrete time derivative of x_1. This system dynamics consists of plant dynamics and a designed controller, such that:

$$x_1(t,k) = [\xi^T(t,k), \zeta^T(t,k)] \tag{5.4}$$

where $\xi(t,k)$ is the plant state and $\zeta(t,k)$ is the controller compensator state. On the other hand, the network influence of M is analyzed using the derivative with respect to k:

$$\Delta x_2(t,k) = g(x_1(\tau(t,k), n(t,k)), t, k) - x_2(t,k-1) \tag{5.5}$$

This network influence does not usually propagate in the network dimension, hence eliminating $-x_2(t,k-1)$. Reaching consensus depends on the network topology for communications among agents, which is described using $n(t,k)$. The topology is fixed if $n(t,k)$ does not depend on t, switching if it varies with t taking values from a finite set, and time-varying if it varies otherwise.

5.3.1 Fixed Topologies

In a fixed topology, a network of single-integrator agents achieves consensus if the graph is connected (undirected network) or strongly connected and balanced (directed network). Furthermore, with constant weights, consensus is achieved for a directed network of single-integrators or double-integrators if the graph contains a spanning tree. Further research has also dealt with consensus in cyclic graphs and cactus graphs[2].

5.3.2 Switching Topologies

Switching topologies are non-fixed topologies where edges may be added or removed from the graph under varying circumstances, hence switching between elements of a finite set of graphs, contrary to time-varying topologies where an infinite set of arbitrary graphs is considered. A switching graph can be represented as:

$$\mathscr{G}_{\zeta(t)} = \{\mathscr{V}, \mathscr{E}_{\zeta(t)}\} \tag{5.6}$$

where it consists of a node set $\mathscr{V} = \{1,2,...,n\}$ and a time varying edge set $\mathscr{E}_{\zeta(t)} \subseteq \mathscr{V} \times \mathscr{V}$, where $\zeta(t)\colon [0,\infty) \to \mathscr{H}$ is piecewise constant and the set $\mathscr{H} = \{1,2,...,\hbar\}$ includes all possible graphs ($\hbar$ is some positive integer), s.t. the graph switches at discrete time instances. Average consensus can be asymptotically achieved for a network of single-integrators with switching topologies taken from a finite collection of strongly connected and balanced directed graphs. Ren and Beard (2005) have also shown that consensus can be achieved if the union of the collection of interaction graphs over some time has a spanning tree frequently enough.

5.3.3 Time-varying Topologies

A particularly interesting problem with time-varying topologies are agents following the 'nearest neighbor rule'; i.e., agents that interact with agents within a limited sensing radius, hence having an undirected graph topology. Jadbabaie et al. (2003) show that discrete-time linearized

[2] graphs where a pair of distinct simple circuits have at most one common vertex

network of such autonomous agents achieves consensus if the joint connectivity condition is satisfies; i.e., if there exists an infinite sequence of continuous, non-empty and bounded time-intervals such that the union of the collection of graphs across each time interval is connected. Furthermore, Tanner et al. (2003) prove that such a network of continuous-time double integrators achieves consensus regardless of switching as long as the graph remains connected.

5.4 Attitude Synchronization in Communication Networks with Switching Topology

Attitude synchronization is the problem of bringing multiple spacecraft attitudes into an agreement; i.e., aiming to maintain the relative attitude between spacecraft in a predefined way (Yu et al. (2019)). This lies in contrast to attitude tracking where multiple spacecraft track a common reference as a virtual leader in a cooperative way, where this reference is only available to a portion of spacecraft (Ren (2010)). While the latter is useful for our application of attitude consensus, the former can perform the same task at lower complexity of control with the only extra requirement for the central spacecraft to be capable of maintaining its attitude with respect to the earth-centered inertial frame of reference.

In most cases, control algorithms proposed for the attitude synchronization problem are applicable only using fixed network topology; i.e., each initial communication link between distinct spacecraft is maintained all the time. This will not be possible in our problem due to the exchanges and rotations of the formation layers and hence it is required to develop coordinated attitude control algorithms using switching topologies. Although previous research involving switching topologies has required switching between (quasi-strongly) connected subgraphs[3], Liu et al. (2020) proves the validity of the consensus algorithm for switching topology that satisfy uniform joint connectivity (for synchronization) or uniform joint quasi-strong connectivity (for tracking), hence allowing spacecraft to lose contact with others for some time. As a result, it is possible for spacecraft to perform attitude synchronization via consensus even before reaching the unorganized pre-assembly stage (i.e., positional convergence), and following positional convergence, attitude synchronization is guaranteed.

Consider a group of n spacecraft, each of whose orientation in the body-fixed frame $\mathscr{B}_i$ is rep-

[3] each spacecraft has a connection link with at least one of its neighbors all the time

resented with respect to an inertial frame $\mathscr{I}$ by the three Tait-Bryan angles for yaw ψ_i, pitch θ_i, and roll ϕ_i, and rotation matrix R_i represents the rotation from $\mathscr{B}_i$ to $\mathscr{I}$. The coordinated attitude synchronization problem requires developing a distributed control algorithm such that all the spacecraft attitudes $p_i = (\psi_i, \theta_i, \phi_i)$ reach a synchronization over a switching network (Liu et al. (2020)):

$$\lim_{t\to\infty}(p_i(t) - p_j(t)) = 0, \ \lim_{t\to\infty}\omega_i(t) = 0, \quad \forall \ i, j \in \mathscr{V} \tag{5.7}$$

The switching graph is assumed as undirected and uniformly jointly connected. Now, the spacecraft formation does not require all attitudes to be equal to each other but to be equal to some predefined attitude exclusively defined for the spacecraft with respect to the attitude of the central spacecraft in terms of its position in its present layer and its final layer number. Due to the initial assumption that the central spacecraft is capable of measuring its own attitude in the inertial frame of reference, it will be capable of maintaining its own attitude at the predefined value; i.e. $(0.0, 0.0, 0.0)$. Other spacecraft will follow the above rule where, instead of representing the actual spacecraft attitude, p_i is given as $p_i = q_i - q_{i,f}$ where q_i is the spacecraft attitude and $q_{i,f}$ is the required attitude that it needs to reach. Here, each spacecraft follows the following consensus law:

$$p_{i,n+1} = \sum_{j\in\mathscr{N}_i} a_{ij}\left(p_{i,n} - p_{j,n}\right) \tag{5.8}$$

where $\mathscr{N}_i$ represents the neighborhood of the spacecraft i. This can also be written in terms of the actual spacecraft attitudes as:

$$q_{i,n+1} = \sum_{j\in\mathscr{N}_i} b_{ij}\left(\left(q_{i,n} - q_{i,f}\right) - \left(q_{j,n} - q_{j,f}\right)\right) \tag{5.9}$$

This law stands independent of whether q_i and q_j are measured in the inertial frame or in the body frame since the subtraction $q_i - q_j$ will cancel the extra element that arises due to the transformation. Hence, spacecraft i is not required to know its attitude or the attitude of its neighbors in the inertial frame. It suffices for the spacecraft to be capable of detecting the attitude of its neighbors with respect to its own body frame.

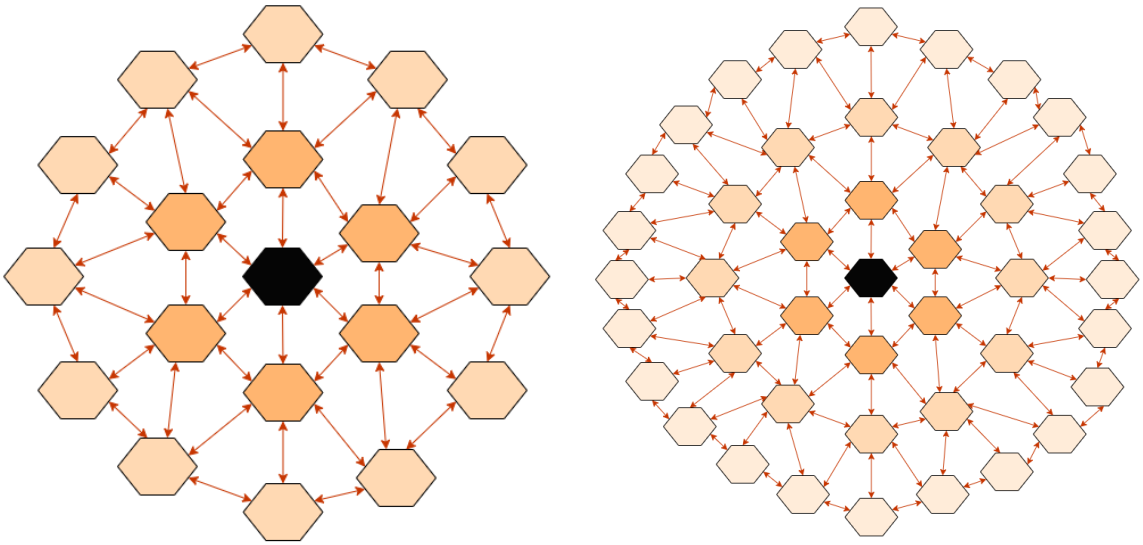

(a) 2 Layers (b) 3 Layers

Figure 5.1: Communication Topology

We now implement this consensus law for the spacecraft formation. The communication topology is depicted in Fig. 5.1. Although this remains stationary, each individual spacecraft need not have the same neighborhood due to layer rotations and exchanges that are performed to reach the final arranged pre-assembly as explained in Section 4.5. As a result, we obtain the result as shown in Fig. 5.2 with suitably chosen values for the weights of the system.

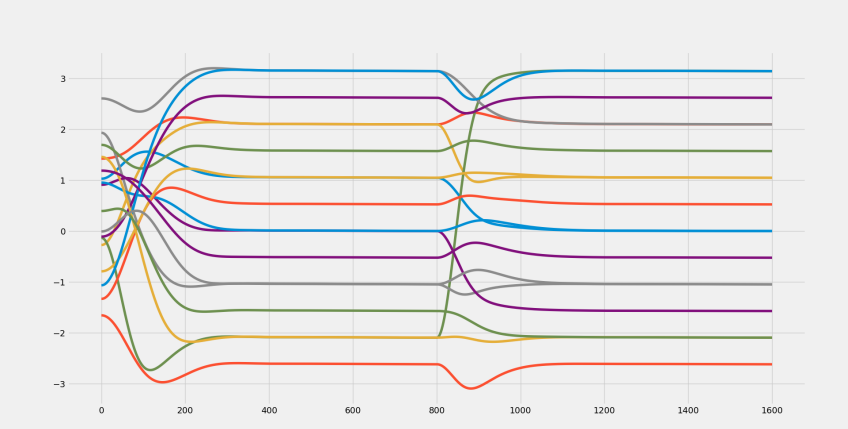

(a) Yaw ψ_i

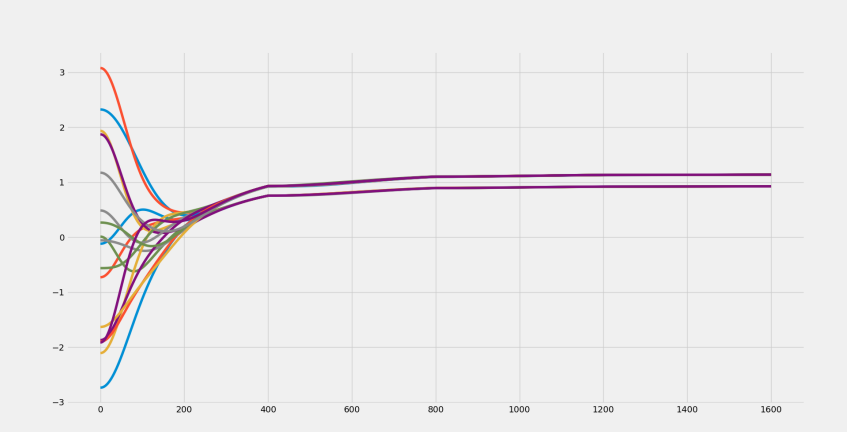

(b) Pitch θ_i

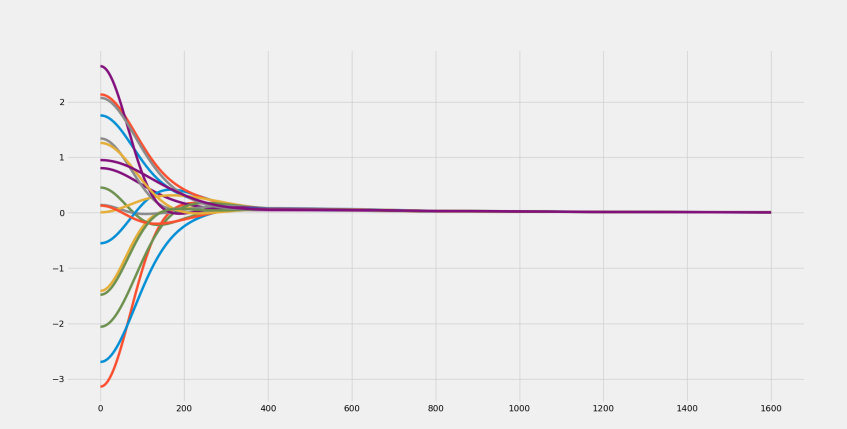

(c) Roll ϕ_i

Figure 5.2: Attitude Consensus

The roll of all spacecraft is set to zero since all segments of the telescope should be capable of docking along a line (edge of a hexagon for the JWST design). Secondly, there are two values for pitch, each of which correspond to a layer of the formation (greater θ implies higher layer number). For a spacecraft on the layer l, this is equal to the angle $\phi_l = \frac{\pi}{2} - \theta_l$ from Fig. 4.4. The yaw of a spacecraft on the layer l (with $numLayerAgents$ spacecraft in the layer) at position i is given by the angle $\frac{2\pi i}{numLayerAgents}$. We observe from Fig. 5.2a that there is a transition in the yaw of two spacecraft after reaching the first consensus. This is due to the IFMEA rotation-exchange process that occurred right before the transition. This change is not reflected in the roll since it is zero for all spacecraft and not in the pitch since each spacecraft aligns itself to the pitch corresponding its own geometry right after positional convergence irrespective of its present layer number.

5.5 Summary

This chapter has introduced some aspects of attitude dynamics, especially the three commonly used rotations: 'yaw', 'pitch', and 'roll'. Following a presentation of previous work on multi-agent control, the concept of attitude synchronization is discussed considering a switching communication topology. We have implemented a corresponding control law in the spacecraft formation framework wherein the above mentioned rotations are defined with respect to the actual layer number and present location of each spacecraft. Here, we incorporate from previous research that attitude synchronization is convergent in switching topologies and, since the communication graph is fixed once all spacecraft attain their final positions, they will converge to the attitude dictated by their positional characteristics.

Chapter 6

Final Remarks

6.1 Conclusion

In this research, we have developed a framework to construct a large telescope in orbit via decentralized control of multiple spacecraft that each host a segment of the telescope. This pipeline deals with the convergence of both the position and the attitude of all spacecraft to values computed based on their physical convergence and final position. Following the spacecraft's position and attitude convergence to the organized pre-assembly stage, we propose that they eject tethers similar to the proposal by Foust et al. (2017) and dock with each other. Finally, the tethers will be pulled back, hence drawing the spacecraft closer and hence effectively forming the telescope.

While tether-based autonomous rendezvous and docking are useful for telescope assembly, they can also be utilized (as suggested by Roa et al. (2017)) for other applications such as space station assembly (with fewer instrument disturbances and higher structural integrity), starshade assembly, construction of space infrastructure, and deployment of giant and more sensitive antennae (for high communication speeds). The algorithms proposed in our research can be suitably modified to match the requirements of the mission. The fields of spacecraft forma-

tion flying and in-orbit decentralized construction have been dealt with in research for several years. We look forward to the materialization of this concept and the subsequent development of human colonization in space.

6.2 Future Prospects

As noted in Chapter 2, the conversion of time anomaly to time has no analytical solution and hence incorporates an approximation. This conversion is valid for our problem due to the short period of operation; however, a superior conversion technique needs to be adopted for more prolonged problems for which the solution time is comparable to the orbital period.
Secondly, while the glideslope rendezvous algorithm has been adopted in our research for the translation of spacecraft to their target locations, further research based on this concept (Ariba et al. (2016), Ariba et al. (2018)) primarily dealing with minimization of fuel have inadvertently developed a solution to constrain the motion of a spacecraft within a rectangular corridor as depicted in Fig. 6.1 and hence prevent collisions with neighboring spacecraft. While we have not accounted for the physical size, this research may be used to consider the same and prevent neighboring spacecraft from approaching within a certain distance until the stage of tethered docking.

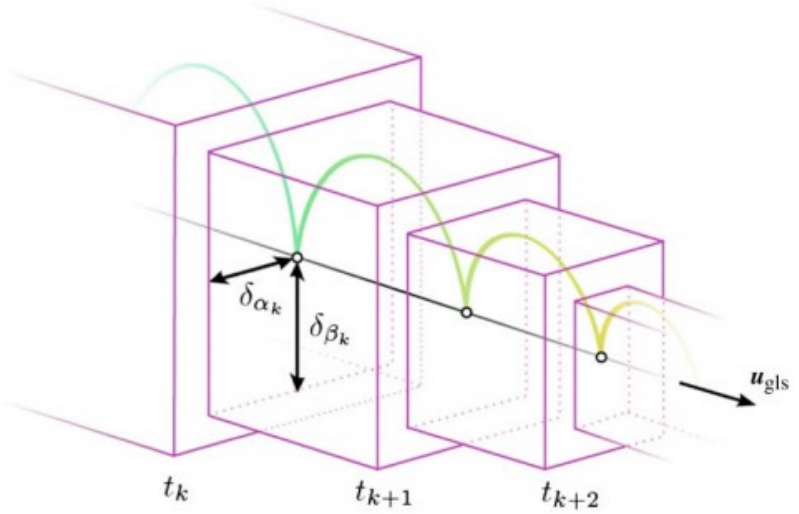

Figure 6.1: Rectangular Corridor of Decreasing Width (Ariba et al. (2018))

Finally, we had noted in Chapter 3 that a hybrid algorithm consisting of the distributed greedy

algorithm until the graph is complete and the ZSP auction algorithm after that will optimize the trajectory of all spacecraft. However, when the spacecraft are far from each other, the central spacecraft, which was previously considered to contain powerful communication systems, may be limited in capability and may not send multiple signals with very high intensity to all the spacecraft due to distance-based constraints. In such a scenario, prior to using the greedy algorithm, the spacecraft system may adopt some form of broadcast control wherein a single command from the central spacecraft is used by all spacecraft to move closer. This technique has been suggested for homogeneous agents by Das and Ghose (2009). The work performed by this research will suffice for our application since IFMEA will be performed after attaining the unorganized pre-assembly positions.

Alternatively, although our research has considered the LVLH frame of a centralized spacecraft to consider collision avoidance, the spacecraft may adopt decentralized frames of reference when they are farther away from each other. Hence, each spacecraft moves closer to its neighbors, and subsequently, the distances between them decrease. The centralized LVLH frame method should be restored when the inter-spacecraft distances are small to prevent collisions between spacecraft that follow different reference frames.

Appendix A

Comparison of the Algorithms used for Positional Convergence

In the following figures, ‘Hungarian Algorithm’ refers to the ‘Distributed Hungarian Algorithm’, ‘Greedy Algorithm’ to the ‘Distributed Greedy (Handshake) Algorithm’, and ‘Distributed Algorithm’ to the ‘ZSP Auction Algorithm’.

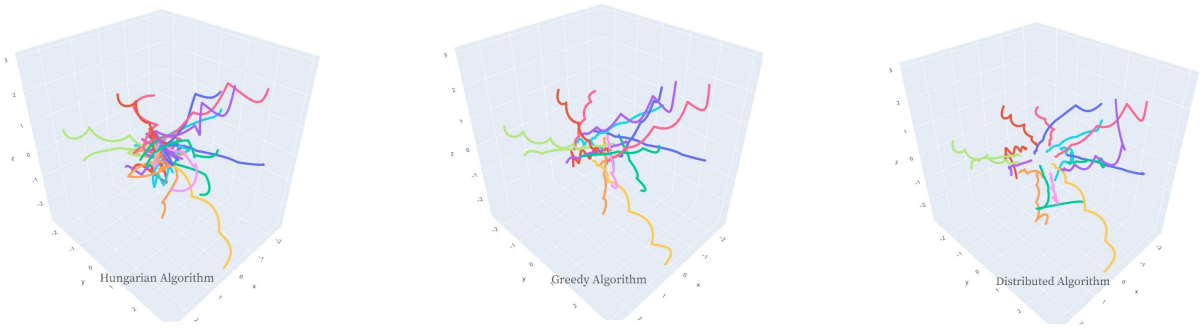

(a) High communication capability

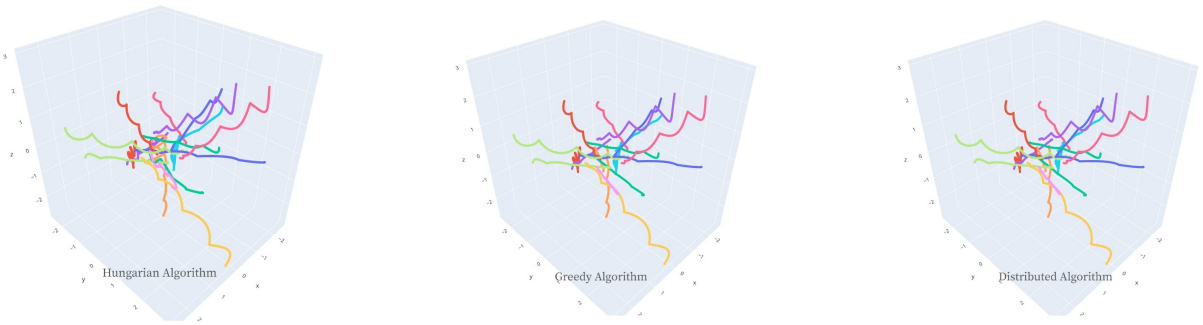

(b) Medium communication capability

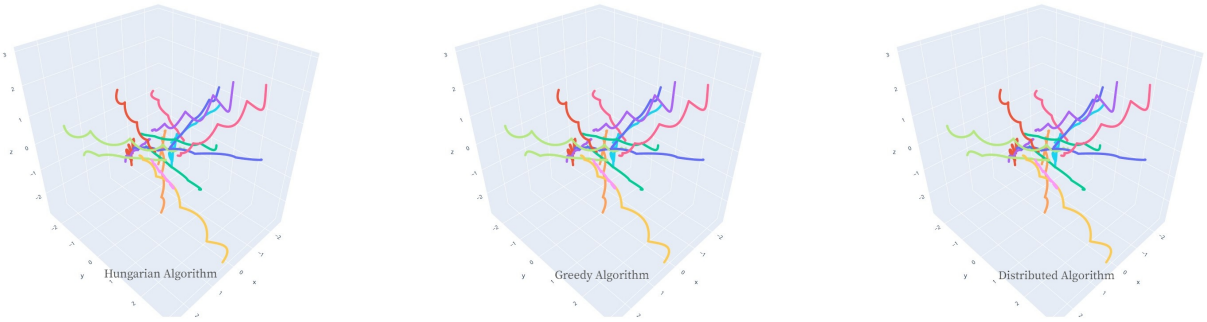

(c) Low communication capability

Figure A.1: Comparison of the Algorithms: Case A

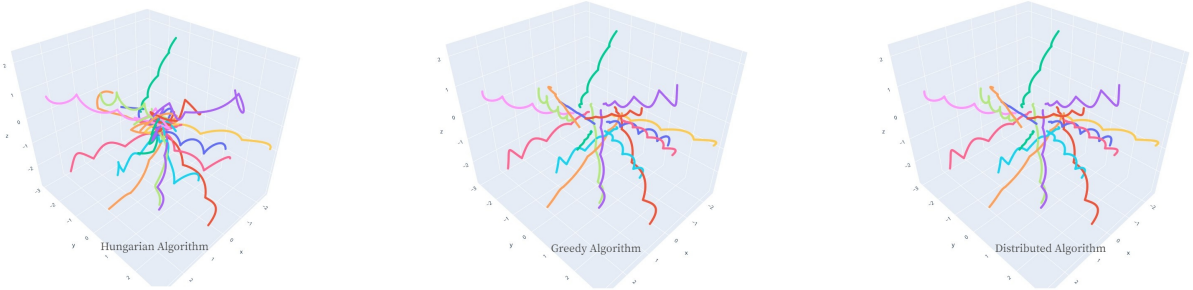

(a) High communication capability

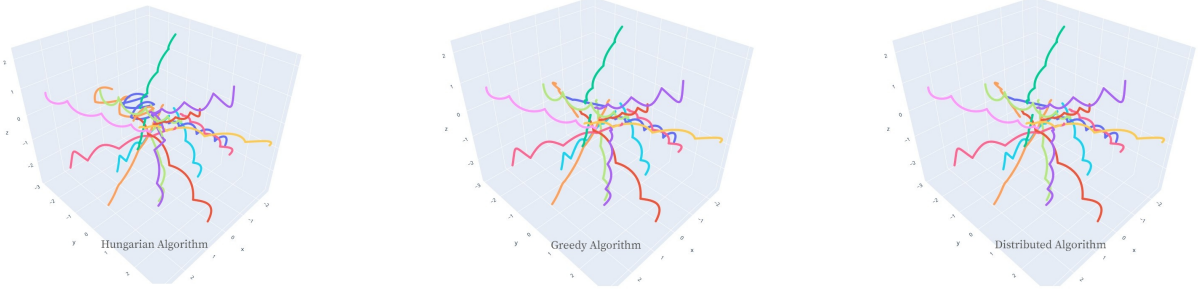

(b) Medium communication capability

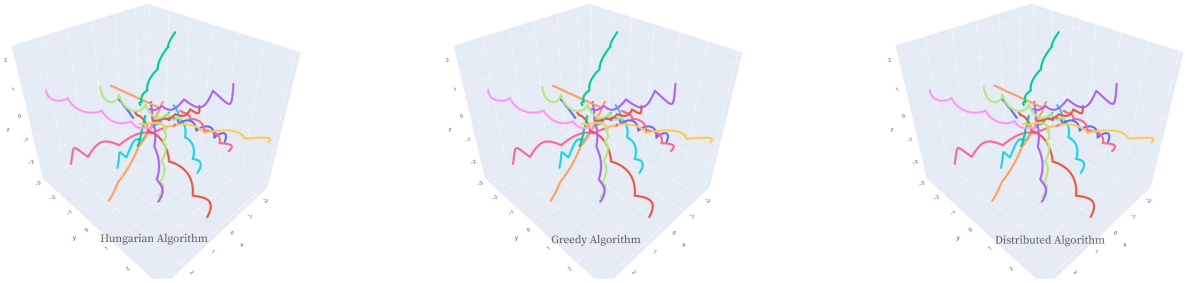

(c) Low communication capability

Figure A.2: Comparison of the Algorithms: Case B

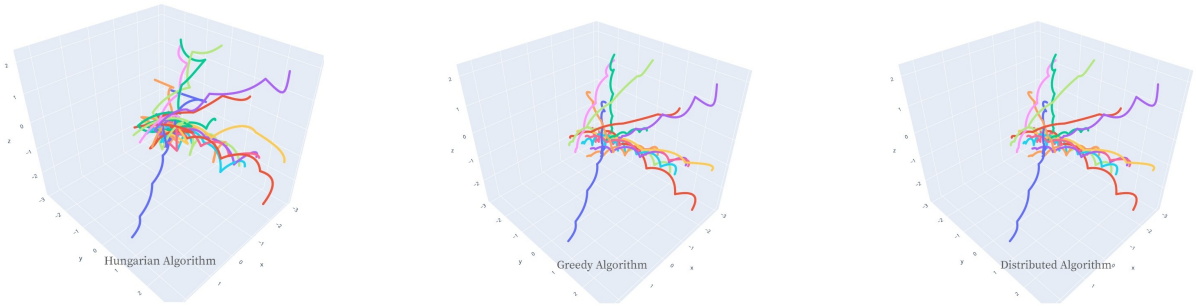

(a) High communication capability

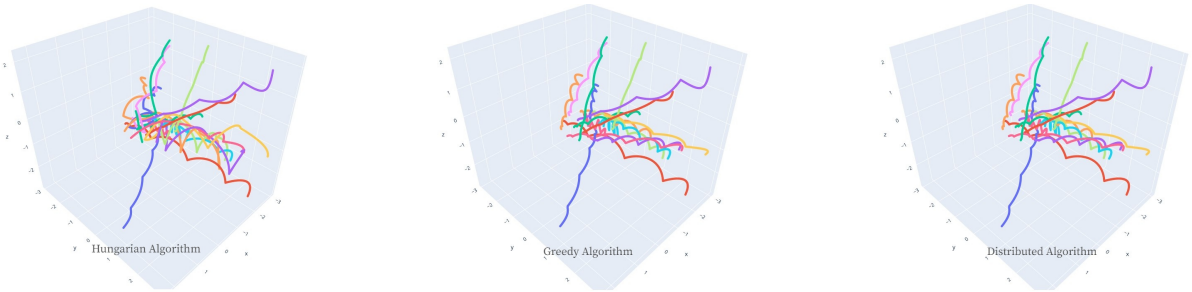

(b) Medium communication capability

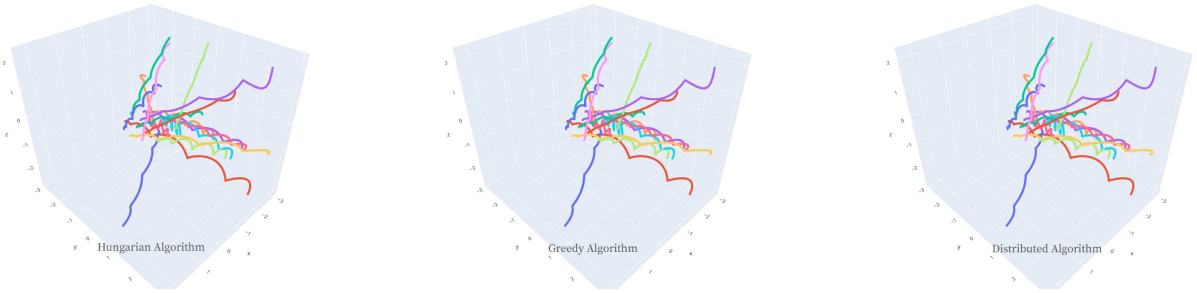

(c) Low communication capability

Figure A.3: Comparison of the Algorithms: Case C

References

[1] Alfriend, K., Vadali, S., Gurfil, P., How, J., Breger, L., 2009. Spacecraft Formation Flying: Dynamics, Control and Navigation. Butterworth-Heinemann.

[2] Ariba, Y., Arzelier, D., Urbina, L.S., Louembet, C., 2016. V-bar and R-bar Glideslope Guidance Algorithms for Fixed-Time Rendezvous: A Linear Programming Approach. IFAC-PapersOnLine 49. doi:10.1016/j.ifacol.2016.09.066. 20th IFAC Symposium on Automatic Control in Aerospace.

[3] Ariba, Y., Arzelier, D., Urbina, S., 2018. Minimum-Fuel Fixed-Time Impulsive Elliptic Glide-Slope Guidance Algorithms Using Semidefinite Programming. Journal of Guidance, Control, and Dynamics 41. doi:10.2514/1.G003395.

[4] Bely, P., 2003. The Design and Construction of Large Optical Telescopes. Springer-Verlag. doi:10.1007/b97612.

[5] Bertsekas, D.P., 1979. A new algorithm for the assignment problem. Mathematical Programming 21. doi:10.1007/BF01584237.

[6] Bertsekas, D.P., Castañon, D.A., 1991. Parallel synchronous and asynchronous implementations of the auction algorithm. Parallel Computing 17. doi:10.1016/S0167-8191(05)80062-6.

[7] Bloise, N., Capello, E., Dentis, M., Punta, E., 2017. Obstacle Avoidance with Potential Field Applied to a Rendezvous Maneuver. Applied Sciences 7. doi:10.3390/app7101042.

[8] Chen, T., Wen, H., Hu, H., Jin, D., 2017. On-orbit assembly of a team of flexible spacecraft using potential field based method. Acta Astronautica 133. doi:10.1016/j.actaastro.2017.01.021.

[9] Choi, H., Brunet, L., How, J.P., 2009. Consensus-Based Decentralized Auctions for Robust Task Allocation. IEEE Transactions on Robotics 25. doi:10.1109/TRO.2009.2022423.

[10] Dang, Z., 2017. Solutions of Tschauner–Hempel Equations. Journal of Guidance, Control, and Dynamics 40. doi:10.2514/1.G002774.

[11] Das, D.K., Ghose, D., 2009. Positional consensus in multi-agent systems using a broadcast control mechanism. Proceedings of the American Control Conference doi:10.1109/ACC.2009.5160384.

[12] Duzzi, M., Olivieri, L., Francesconi, A., 2016. Tether-aided Spacecraft Docking Procedure .

[13] Fehse, W., 2003. Automated Rendezvous and Docking of Spacecraft. Cambridge University Press. doi:10.1017/CBO9780511543388.

[14] Foust, R.C., Lupu, E.S., Nakka, Y.K., Chung, S.J., Hadaegh, F.Y., 2020. Autonomous in-orbit satellite assembly from a modular heterogeneous swarm. Acta Astronautica 169. doi:10.1016/j.actaastro.2020.01.006.

[15] Foust, R.C., Nakka, Y., Saxena, A., Chung, S.J., Hadaegh, F., 2017. Automated Rendezvous and Docking Using Tethered Formation Flight .

[16] Goldstein, H., Poole, C., Safko, J., 2000. Classical Mechanics. Addison-Wesley. 3 ed.

[17] Greenhouse, M., 2019. The James Webb Space Telescope: Mission Overview and Status doi:10.1109/AERO.2019.8742209.

[18] Hablani, H.B., Tapper, M.L., Dana-Bashian, D.J., 2002. Guidance and Relative Navigation for Autonomous Rendezvous in a Circular Orbit. Journal of Guidance, Control, and Dynamics 25. doi:10.2514/2.4916.

[19] Han, J.Y., Lee, S., Kim, D.W., 2019. Parametric geometry analysis for circular-aperture off-axis parabolic mirror segment. Journal of Astronomical Telescopes, Instruments, and Systems 5. doi:10.1117/1.JATIS.5.2.024010.

[20] Jadbabaie, A., Jie Lin, Morse, A.S., 2003. Coordination of groups of mobile autonomous agents using nearest neighbor rules. IEEE Transactions on Automatic Control 48. doi:10.1109/TAC.2003.812781.

[21] Jin, J., Park, B., Park, Y., Tahk, M.J., 2006. Attitude control of a satellite with redundant thrusters. Aerospace Science and Technology 10. doi:10.1016/j.ast.2006.04.005.

[22] Knorn, S., Chen, Z., Middleton, R.H., 2016. Overview: Collective Control of Multiagent Systems. IEEE Transactions on Control of Network Systems 3. doi:10.1109/TCNS.2015.2468991.

[23] Kuhn, H.W., 1956. Variants of the hungarian method for assignment problems. Naval Research Logistics Quarterly 3. doi:10.1002/nav.3800030404.

[24] Kuhn, H.W., Yaw, B., 1955. The Hungarian method for the assignment problem. Naval Res. Logist. Quart .

[25] Liu, X., Zou, Y., Meng, Z., You, Z., 2020. Coordinated Attitude Synchronization and Tracking Control of Multiple Spacecraft Over a Communication Network With a Switching Topology. IEEE Transactions on Aerospace and Electronic Systems 56. doi:10.1109/TAES.2019.2925512.

[26] Lusk, P.C., Cai, X., Wadhwania, S., Paris, A., Fathian, K., How, J.P., 2020. A Distributed Pipeline for Scalable, Deconflicted Formation Flying. IEEE Robotics and Automation Letters 5.

[27] McLean, I.S., 2008. Electronic Imaging in Astronomy: Detectors and Instrumentation. Springer-Verlag Berlin Heidelberg. doi:10.1007/978-3-540-76583-7.

[28] Melton, R.G., 2000. Time-Explicit Representation of Relative Motion Between Elliptical Orbits. Journal of Guidance, Control, and Dynamics 23. doi:10.2514/2.4605.

[29] Oswalt, T., McLean, I.S., 2013. Planets, Stars and Stellar Systems - Volume 1: Telescopes and Instrumentation. Springer Netherlands.

[30] Ren, W., 2010. Distributed Cooperative Attitude Synchronization and Tracking for Multiple Rigid Bodies. IEEE Transactions on Control Systems Technology 18. doi:10.1109/TCST.2009.2016428.

[31] Ren, W., Beard, R.W., 2005. Consensus seeking in multiagent systems under dynamically changing interaction topologies. IEEE Transactions on Automatic Control 50. doi:10.1109/TAC.2005.846556.

[32] Roa, M.A., Nottensteiner, K., Wedler, A., Grunwald, G., 2017. Robotic Technologies for In-Space Assembly Operations .

[33] Roy, A., 2004. Orbital Motion. CRC Press.

[34] She, Y., Li, S., Liu, Y., Cao, M., 2020. In-orbit robotic assembly mission design and planning to construct a large space telescope. Journal of Astronomical Telescopes, Instruments, and Systems 6. doi:10.1117/1.JATIS.6.1.017002.

[35] Sidi, M.J., 1997. Spacecraft Dynamics and Control: A Practical Engineering Approach. Cambridge Aerospace Series. doi:10.1017/CBO9780511815652.

[36] Tanner, H.G., Jadbabaie, A., Pappas, G.J., 2003. Stable flocking of mobile agents - Part I: Dynamic Topology 2. doi:10.1109/CDC.2003.1272911.

[37] Terzakis, G., Lourakis, M., Ait-Boudaoud, D., 2018. Modified Rodrigues Parameters: An Efficient Representation of Orientation in 3D Vision and Graphics. J Math Imaging doi:10.1007/s10851-017-0765-x.

[38] Tschauner, J., Hempel, P., 1964. Optimale Beschleunigungsprogramme für das Rendezvous-Manöver. Astronautica Acta 10.

[39] Yamanaka, K., Ankersen, F., 2002. New State Transition Matrix for Relative Motion on an Arbitrary Elliptical Orbit. Journal of Guidance, Control, and Dynamics 25. doi:10.2514/2.4875.

[40] Yu, Y., Liu, W., Yang, Z., Miao, C., Jiang, W., 2019. A Distributed Consensus Protocol for Attitude Synchronization and Tracking of Multiple Spacecraft on Directed Graphs doi:10.1109/ICCA.2019.8899961.

[41] Zavlanos, M.M., Spesivtsev, L., Pappas, G.J., 2008. A distributed auction algorithm for the assignment problem doi:10.1109/CDC.2008.4739098.